nature portfolio

Peer Review File

Sub-second Volumetric 3D Printing by Synthesis of Holographic Light Fields

Corresponding Author: Professor Qionghai Dai

This file contains all reviewer reports in order by version, followed by all author rebuttals in order by version.

Version 0:

Reviewer comments:

Referee #1

(Remarks to the Author)
The manuscript by Xukang Wang and coworkers reports an important accomplishment in the field of volumetric 3D printing. The authors are to be congratulated and commended on their impressive demonstration of sub-second volumetric printing, the capability to print through a flat interface deep into a volume (rather than requiring 360 deg of optical access around a cylindrical perimeter), the meticulous and careful characterization and calibration of their optical system, and its demonstration with multiple materials and flow-coupled fabrication. These technical achievements are a significant advance in the field of volumetric photopolymer 3D printing (and beyond), and will surely be noted by the community. The experiments are carefully executed, the manuscript is mostly well-written and well-organized, and the results are mostly presented in appropriate detail.
However, for publication in a high-impact journal with an extremely broad readership such as Nature, revisions are necessary to more clearly describe the key principles that allow for these achievements, and place the work more completely into the relevant context. I would recommend acceptance of the manuscript after significant revisions that address the following questions and provide additional details as follows.

OPTIMIZATION OF ABSORBED DOSE

The authors optimize the light fields based on calculating accumulated dose (lines 135-140), and its difference with a high and low threshold. They define "dose" as the product of intensity $I(\vec{x})$ and exposure time Δt. Later, the equation on lines 392 and 404, and associated discussion similarly refer to this type of "dose" calculation. This is incorrect – the product of time and intensity is (areal) radiant exposure (units of mJ/cm^2), appropriate to use in a layer-by-layer printing context, when light is impinging onto a flat layer of resin. When calculating doses in a volumetric context, a volumetric absorption factor must also be included (units of 1/cm), which is derived from the resin absorbance. I would recommend reviewing the supplements of Tumbleston et al [ref 13 of this manuscript] or following the approach of references [17] or [18] for calculations of volumetric absorbed dose. Refer also to Pritchard et al https://doi.org/10.1002/admt.201900700 where volumetric dose estimation is appropriately reported with layered printing as well. This fundamental misconception must be corrected, so that dose can be calculated/optimized in appropriate physical units of mJ/cm^3.

UNCLEAR HOW AND WHY HOLOGRAPHIC LIGHT FIELDS ENABLE THE REPORTED RESULTS:
The authors emphasize the importance of their use of a coherent laser source, and the use of holographic light fields to expose the resin. The conventional understanding of holographic light projection involves the shaping/control of both the amplitude and phase of the light. Yet, the pattern generating device used here is a DLP9500 (manuscript line 303), which controls only amplitude, and the authors' only mention of optical phase is on line 414-415, to say that the "phase is constant" in their optimization. The authors model light propagation using complex fields in a wave-optics approach (lines 127-147, and 327-349), and this appears to be a correct and fully-holographic description of the system (note also the recent paper from Wechsler et al reporting a wave-optical mode https://doi.org/10.1364/OE.521322 which should be cited). However, if their hardware is not applying any phase-shaping to the optical pattern, and the phase profile of the source laser is not being measured or controlled, and the phase is a constant in the complex propagation optimization, why is holographic (complex amplitude) necessary at all? Why must the holographic light fields be incoherently synthesized (i.e. their intensities superimposed, but phase interference is not part of the picture)? This needs to be more clearly explained. The trade-off for this approach is computational expense, with the algorithm taking 24 hours to complete (line 427). Is the trade-off worth the gain in accuracy? The authors do not discuss this.

Additionally, Fig 1d and lines 119-124 emphasize the benefit of a coherent source, but the authors do not quantify the coherence of their laser. Please provide either the spectral bandwidth or the coherence length of the laser. Lastly, coherent sources inevitably carry with them the drawback of speckle noise, which can significantly degrade printing accuracy, and which must usually be countered by a variety of means. No such noise is discussed or mitigation shown in this manuscript, which is an omission that must be corrected.

THE TRUE ACCURACY/RESOLUTION OF THIS TECHNIQUE IS UNCLEAR
The highest-resolution prints, which are used to demonstrate the 11 µm resolution (Fig 3g and 3h, as well as Figure S11) are only shown as ridges/lines on a much larger bulk slab. Can the authors explain why, for instance, they do not show free-standing structures or other features of similar size? All prints besides these figures show much larger and coarser features, with less-accurate results. The structures in Fig 4 seem to have surface waviness or distortion on a scale of ~100 µm at best (see below). It may be the case that the achievable *optical* resolution of this system reaches 11 µm, and can only reproduce features at that size when textured onto larger objects. But when reaction-diffusion tradeoffs due to the photochemical kinetics come into play, such fine features do not seem to be attainable. This does not invalidate the authors' results, but must be discussed, and cannot be swept under the rug. (Note that similarly, the optical system in Toombs et al (Ref 21) is reported to have a modulation transfer function of ~100 cycles/mm, which would yield a resolution of 5-10 µm, but the structures can only be fabricated with ligaments/elements down to about 50 µm in width).

ADDITIONAL IMPORTANT, BUT LESS FUNDAMENTAL ISSUES TO CONSIDER:
1. The dimensional accuracy of most of the printed structures is difficult to assess (e.g. all structures in Fig 4). Please compare at least once or two final printed structures (not only the modeled dose distributions in Fig 2d and S6, S7) to the original source geometry. A CT scan or laser-based surface scan of a print can provide this information (refer to Ref 25 or Ref 22, or the more recent report from the same group https://doi.org/10.1016/j.addma.2024.104480). {Note, relatedly: please add units to the y-axis of the signed distance plots in Supp Figures 6 and 7}.

2. The discussion of binarization is extremely confusing. It seems that this is a way of overcoming the native pulse-width-modulated (PWM) method that the DMD typically uses to generate grayscale images. The authors instead seem to be generating binary image-sets at various bit-depths to encode the grayscale intensity maps calculated by the algorithm. Why this must be done *inside* the optimization loop and then projected using the wave-optics operators is not clear, nor how this improves the results of the optimization. For instance, why not run the optimization loop on the complex-valued field, and only run binarization after the optimization completes?

3. The authors claim "low viscosity" on lines 34 and 110 but the viscosities are not reported. Please measure and report viscosities of the various resins. Viscosity is a critical parameter in volumetric 3D printing and it is important for comparison with other investigations in the field.

4. In the Abstract, the authors mention "a tradeoff between precision and efficiency" (lines 23-24) implying that this work moves beyond that trade-off (a better way to describe the trade-off is between resolution and volumetric build rate). This is not quite convincingly demonstrated. Supplementary Figure 1 is meant to illustrate this, and manuscript lines 273-276 mention some metrics about throughput. Why is the addressable volume only 200 mm^3 when line 426 later says that the addressable volume is 7.3x7.3x10 mm = 533 mm^3? And the voxel size given on line 275 indicates that the voxels of this approach are rhomboidal (not parallelepipedal). This needs to be discussed further, to support the claim of going beyond the resolution/build rate trade-off. Supplementary Figure 1 would be more informative and convincing if the axes were switched (minimum feature size on the x-axis, throughput on the y-axis) and the "scanning and exposure time" metric were converted to volumetric build rate (mm3/s), similarly to figures from Hahn et al https://doi.org/10.1002/adfm.201907795 and https://3dprintingspeed.com or Wirth et al https://doi.org/10.1016/j.addma.2024.104081

REQUESTED MINOR CHANGES:

-- The abstract claims "massive [sic] continuous flexible production" (what is meant, I think, is mass fabrication or mass production). However, Supplementary Video 2 makes clear that structures are produced in a stop-flow mode, at a rate of ~0.2 Hz. This is a fine approach, but to describe this as "continuous" is inaccurate. Can the authors comment on a maximum possible rate? Although Figure 4c shows a handful of structures, this is not yet at "mass fabrication" throughput; being able to show e.g. 10s or 100s of objects would be preferable before claiming mass fabrication.

-- In Fig 3g (and in Supplementary Fig 11), please indicate by overlay or arrows which were the relevant stripe patterns and what their designed dimensions are (compared to the measured 54, 11, 15.5, 20.9 and 33.1 µm line widths).

-- Please add units for signed distance calculations of Supplementary Figures 6 and 7.

-- In Supplementary Figure 6a and 6b, the panels are labelled "intensity of the cross-sections" where I think dose distribution is meant. Again the difference between a 2D optical pattern and a 3D volumetric quantity is being confused here.

-- In Supplementary Fig 8, some of the text is too small to read, please increase the size.

-- Lines 503-513 describing the 3D display capability, together with the Supplementary Figure 13 seem a little out of place. This is a nice additional capability but ultimately not related to the main point of the paper. I recommend removing it, unless they are critical to understanding other parts of the printing/calibration process.

Referee #2

(Remarks to the Author)
The scope of this paper is a volumetric projection technique termed digital incoherent synthesis of holographic light fields (DISH) and its use in additive manufacturing. This concept builds on volumetric projection techniques, most notably computed axial lithography (CAL) which is the current state-of-the-art in volumetric printing. On of the trade-offs in CAL is the fact that the volumetric projection reconstruction requires the illumination under various angles which is generally implemented by rotating the sample while leaving the projection source (usually a dynamic light patterning device such as digital micromirror device, DMD) stationary. This is the de facto gold standard given that the rotation of the light source is, instrumentally speaking, significantly more challenging. This sacrifices speed for commodity. As speed emerged as one of the most important criteria in volumetric additive manufacturing (VAM), the community investigated methods for speeding up the technique further. Various concepts have been explored and (at least theoretically) described. The technique presented in this work uses a rotating periscope. While this approach has been mentioned, the reviewer is not aware of an actual implementation and certainly not at the time scales demonstrated in this work.
To make one point very clear: This paper is an impressive improvement over the current state-of-the-art and merits publication in Nature. There are a couple of points which should be added and/or complemented in order to strengthen some aspects of the work.
It would be good to include a measure of achievable precision. This is still a major point of concern in VAM and has been at the center of attention of the community. In general, we found that precision requires more gentle and extended illumination in order to achieve contrast. DISH is very fast and thus, it would be important to gauge, how precise the structures produced can be. This is particularly true as the examples given (including the videos)

show components which are convectively moved during polymerization and thus, the precision does not only depend on the illumination but also the ambient transport conditions (convective ad- and off-transport of monomers, etc.). In order to assess this, it would be good to generate a test pattern with defined geometries. This pattern should be printed and measured to assess achievable precision and resolution. Mind you, it is not necessary to do this volumetrically, i.e., using tomography or the likes. A simple 2D test pattern (which can be checked using a microscope) would be entirely sufficient.
The structures shown do not feature sharp edges. All hard corners seem rounded off. All images in Fig. 4 seem organic, even the airplane has rounded corners where the digital model would have a hard edge. It would be good to assess, how well DISH can produce hard edges and intended angles (30deg, 45deg, etc.). Again, a sample structure would be sufficient her.
Please indicate the irradiance (i.e., intensity per area) of the light source as well as the beam profile emitted from the DMD. For this, an intensity scan (in the easiest sense with a CMOS or CCD chip) should be recorded on the DMDs projection beam when the DMD is set to all white. It would be important to know how uniform the projection needs to be.
Please elaborate on the need for the improved algorithm for the generation of the phase projection patterns. Obviously, the strength of the GS algorithm is neither its speed nor the chance of converging to a global maximum. It is used for its numerical stability (i.e., it is near-impossible to nor converge GS) as well as the fact that convergence can be proven, i.e., the algorithm will (almost) always find an optimum - even if its only a local one. Lastly, FFT and iFFT are fast and very convenient to scale on commodity hardware which makes GS optimization affordable. How does this algorithm compare in terms of stability and cost (i.e., what is the big O scaling of the algorithm?)? How long does pattern prepreparation take and which hardware is required? This is still a bottleneck in conventional CAL as the time needed to derive the sinograms is significantly longer than, e.g. a slicer would take.
I would also tune down the claim on diverse materials. All of the materials shown are all (meth)acrylates. In order to claim diverse materials, it would be necessary to add also ionic materials (such as, e.g., epoxy-based), thiol-ene or other type of additive-type polymers. This is not a major point of concern, VAM currently mostly investigates acrylates - but this is not a particular achievement of this paper and thus, this claim should either be complemented or tuned down.
In summary: This is an impressive piece of work which merits publication after the given points have been amended.

Referee #3

(Remarks to the Author)
The manuscript by Wang et al., titled "Sub-second Volumetric Additive Manufacturing by Digital Incoherent Synthesis of Holographic Light Fields" is timely and aligns with the significant progress made since the development of computed axial tomography (CAT), xolography, and acoustic field-based techniques for volumetric 3D printing. The method shares striking similarities with CAT, where pre-calculated 2D light patterns are projected into a volume to generate a targeted 3D light dose that induces photopolymerization within the desired region. However, instead of rotating the vat to allow radiation from different angles, the light beam is directed by a rotating periscope system, which enables it to enter from various orientations, while the vat remains stationary. This enables faster application of the angular projections and thus printing with low-viscosity resins, where the objects would otherwise be deformed by gravitational sinking. Although the movement of the optical components poses a challenge for the precise superimposition of the individual projections in the cuvette, the authors were able to solve these problems through fluorescence imaging and the use of adaptive optics. They pursue the approach of radiating several projections for each angular range in order to generate structures with higher resolution outside the depth of field of the objective. Wave-optical modelling and iterative algorithms are developed to optimize angular projections. Supplementary video 1 and 2 show the fast object creation and 3D printing in the flow.

The method is based on the principles of CAT, so its novelty is not particularly groundbreaking. Additionally, the paper currently lacks sufficient data and results, so I do not recommend publishing it directly in Nature. However, if the points discussed below are effectively addressed in a major revision, I would support its publication in one of the sub-journals of the Nature portfolio, as the results could be impactful in the field of volumetric 3D printing and of interest to a broader audience.

1) Limited Angle Projections / Missing Cone Problem:
In CAL, the resin vessel is rotated 360 degrees, allowing projections to enter the vat from all directions. This is crucial for ensuring the accuracy and fidelity of the resulting shape. As shown in Suppl. Figure 3, the light beam always enters the cuvette through one of its side windows at a 45-degree angle relative to the surface normal. As the beam rotates, it irradiates a cone that covers a solid angle of about 0.6π in air. In the cuvette, the cone is even smaller, as the light beam is refracted toward the normal line due to the increase in refractive index at the air-cuvette-resin interface.
The authors frequently refer to a "360-degree projection," as stated on page 4, line 71: "…to deliver a 360-degree high-resolution projection of precisely controlled light fields at …," and on line 78: "…then developed to optimize 360-degree holographic patterns …," and line 95: "in DISH to facilitate 360-degree projections," among others. While the periscope makes full rotations, referring to the angular projections as 360 degrees is misleading and should be corrected. It would be valuable to provide a theoretical analysis of how projections from a limited set of angles affect resolution and shape fidelity. Additionally, it would be helpful to explain why a 45-degree angle was chosen instead of a larger angle.
The authors propose an alternative design, shown in Suppl. Fig. 12, to solve the problem of the missing cone, but no further results have been published. As this approach is introduced into the conclusion section, it should be described why this has not been implemented so far and what are the obstacles to realize it.

2) Build-Volume Size:
The superposition of the individual beams, each with a 6mm diameter, within the cuvette defines the build volume within the resin space. Based on the schematic in Suppl. Figure 2, the build volume in the y,z plane resembles a rhombus, which could significantly reduce the available print volume depending on the shape of the object being printed. The authors demonstrate the fabrication of objects, as shown in Figure 1 and Suppl. Figure 10, with dimensions of approximately 7-8mm in the z-axis and a maximum of 3-4mm in the x and y axes. However, they mention the printing of centimeter-scale objects, for example, in the abstract (page 2, line 31), the main text (page 3, line 50), page 4 (line 66), page 7 (line 118), and several other places throughout the manuscript. Based on the demonstrated fabrication sizes, the proposed setup appears to allow printing of millimeter-scale objects only and the manuscript should be updated accordingly. The shape and size of the available build volume are not discussed in detail. On page 4, the manuscript briefly mentions "…the entire 1 cm^3 volume …," while in the conclusion (line 273), it states: "By DISH, a sample with a volume of approximately 200 mm^3 can be produced in …." There is a discrepancy of a factor of 5 between these two values, which should be clarified. It would be helpful to provide the dimensions of the build volume (in the x, y, z axes) as a function of the central design parameters of the periscope and illumination geometry.
What are the main factors that currently limit to increase the build volume?

3) Resolution:
The authors report the printing resolution in the abstract: "… in DISH maintains an 11-µm printing resolution across the 1 cm range." However, on page 11, line 216, they state: "Finally, we quantitatively characterized the experimental printing resolution of DISH at different axial positions by printing high-resolution stripes on the 3D surface. A model with an axial length of 1 cm was designed with featured lines of different widths on the surface, with the

smallest line width of 10.8 μm corresponding to 2 DMD pixels (each pixel corresponds to about 5.4 μm at the objective plane)."
From the description, it remains unclear what type of "3D surface" was printed. The image in Fig. 3g suggests a thin rhombic model to fit the build volume. It appears that this model was deliberately chosen to demonstrate the smallest feature size based on the lateral spacing of DMD pixels, which are directly imaged onto a thin surface (a 2.5D object) without the presence of potentially degrading structures around it. This is not a reference object with extended geometry, and I would suggest fabricating a more representative model, such as a "benchy" model or common 3D resolution targets, including both positive (pins, rods) and negative (holes) features, to provide more convincing data on the achievable x, y, and z resolution.
Ideally, the characterization should be performed using SEM images, micro-computed tomography (CT), or profilometry data sets. Similar to CAL, the resolution seems to degrade as the object size and complexity increase. For example, looking at the other objects printed, as shown in Fig. 1b, they appear quite blurry, and the resolution seems to be significantly lower than 11 μm, likely in the 50-100 μm range.
In this context, the benchmarking of DISH in relation to other methods in Suppl. Figure 1 remains questionable.

4) Shape fidelity and mechanical properties of printed objects:
To better convince the reader of the DISH process's performance, I would recommend including an image of the 3D model (e.g., STL file or similar) in Figure 1b, ideally placed side-by-side with a photograph of the printed object for a direct comparison of shape fidelity.
Throughout the manuscript, I found no information regarding the mechanical stability of the objects after printing and the subsequent post-processing step. The induced crosslinking may be sufficient to remove the object from the resin but might leave the construct soft and unstable. Photographs alone typically do not provide enough insight into this aspect. I suggest including an additional supplementary video that demonstrates the post-cured objects, which would also help visualize shape fidelity.
Furthermore, there is limited information provided in the Methods section on page 24 regarding the post-processing procedure. For instance, details on the irradiance (W/cm^2) and illumination time used during the 405 nm UV post-curing step would be helpful.

5) Holographic optimization
As is well-established from previous CAL studies, extensive modeling and algorithm development are required to compute projections for printing high-resolution, true-to-shape objects.
Based on the description in the Methods section, I assume that the algorithms published in references 25 and 26 are used to calculate coarse image projections (grayscale, real-valued) for N = 180 discrete angles. Is that correct? From each of these images, a set of G = 10 binarized images is generated, which are then processed through the holographic optimization algorithm, resulting in a total of 1800 projection images. Why not calculate projections directly for N = 1800 different angles using traditional algorithms, binarize them, and then feed them into the newly developed optimization algorithm? If the mentioned computation time is the reason for this approach, how long do these computations take to run on the machines used?
Additionally, I was searching for documentation regarding the software implementation of the PM methods and the Gerchberg-Saxton algorithm used in this work. For transparency, it would be helpful to provide more detailed information about the software and its implementation.

6) Other points:
In the introduction on page 3 of the manuscript, the authors wrote: "Efforts have been made on continuous printing to enhance the production rate and reduce the layering structure, such as continuous liquid interface production, Xolography, and their improved versions for continuous production using continuous roll or fluid control. Still, the throughputs of these methods are fundamentally limited by the layer-wise process, especially for millimeter-scale or centimeter-scale objects."
Xolography is not a layer-wise process, as the material volume in relation to the vat remains stationary while the light-sheet moves continuously through the resin, resulting in smooth, highly homogeneous structures. Therefore, Xolography is a form of volumetric additive manufacturing, and this distinction should be reflected in the text.
Figure 1 provides a clear visualization of the illumination geometry (Fig. 1a,b) and a time series of the printing process (Fig. 1c). Fig. 1d displays a fine mesh structure, and at first glance, the reader may assume this is a printed object. However, the figure caption clarifies that it is a simulation. I would suggest that real prints and simulation data of different objects not be mixed within a single figure to avoid any confusion.
The cited literature list is well-constructed. However, a recent review article published in Nature may be worth including:
Bernal, P.N., Florczak, S., Inacker, S. et al. The road ahead in materials and technologies for volumetric 3D printing. Nat Rev Mater (2025). https://doi.org/10.1038/s41578-025-00785-3

Version 1:

Reviewer comments:

Referee #1

(Remarks to the Author)
This manuscript by X. Wang & colleagues improves significantly upon the first submitted version of this paper. The work demonstrates four major advancements for volumetric additive manufacturing (VAM). 1. The fastest VAM print times reported to-date, 2. Optical access from only one side of the print volume, 3. Improved precision using holographic processing of the light fields, and 4. Stop-flow sequential production of dozens of distinct and varied parts.

Once again, I am impressed by the authors' careful, detailed responses to the reviewers and by their extensive characterization and depth of analysis of their system. In my view, the revised manuscript has sufficiently addressed all of the important concerns from all reviewers. From a technical/scientific perspective, the work is a tour-de-force that certainly merits speedy publication.

I will limit my remaining comments here to only those that aim to improve the clarity of the information presented in the manuscript so as to better convey to readers the key insights, conclusions, and impact of this work. I have one major suggestion, and a few minor suggestions.

INCOHERENT HOLOGRAPHIC SYNTHESIS

If I have correctly understood the authors' responses to reviewers, they do not claim that their hardware is capable of phase modulation. The DMD device is controlled to project binary intensity patterns, as is typical. Rather their key insight is that it's important to model the propagating optical fields using full-wave optics including amplitude and phase, and to treat their interaction and interference holographically, taking this into account for optimizing the distribution of light energy. This leads to more accurate dose estimation and better contrast optimization for the projected light fields, in addition to an extended region of precise optical pattern synthesis far outside the depth of focus of the objective. This is a subtle, but critical aspect of this work.

I believe it is important to convey this to readers using more precise language than currently present in the manuscript. There are a few phrases which imply that the hardware system is somehow holographically shaping the light patterns. These include "continuous multi-angle holographic projections" (line 29), "generate holographic patterns" (line 78), "using holographic light fields" (line 122), "operated with holographical patterns" (line 442), "projection of the holographic patterns" (line 732). The conventional understanding of all such phrases is that the hardware is capable of modulating the phase of the projected light fields, thereby generating holographic patterns. I recommend revising each of these phrases to avoid leaving this impression. On line 29, the word "holographic" can be simply omitted, and can be likewise omitted on line 78 as well, or replaced with "binary intensity." On line 122, I would suggest revising to "… we address this problem by using a coherent laser source, and holographically calculating the light fields, which can achieve …. " On line 442, I suggest revising to "holographically synthesized patterns," and on line 732 revising to "… high-speed projection of the light patterns modulated by…."

I would also suggest explicitly stating somewhere (similarly to the authors responses to Reviewer 1) that indeed the hardware does not modulate the phase of the projected patterns, but calculating the propagation and interference of the light patterns holographically is critical to the success of this work. Perhaps this might fit well on line 80, before the sentence starting with "An iterative algorithm…"

OTHER MINOR SUGGESTED REVISIONS

- It would be very helpful to include Figure R6 perhaps in the Supplementary Information, as a clear demonstration of the difference in pattern contrast due to binarization and why it needs to be included in the optimization loop.

- The sentence that begins on Line 34 of the abstract could better be worded as: "Acrylate resins in a range of viscosities are used to demonstrate…

- On line 69, the words "within snapshot" should be deleted.

- "Rounds" on lines 76, 99, and 310 should be replaced by "rotations." While on the topic, what is the actual rotation speed of the periscope during prints? The videos seem to show slower speed than 10 Hz.

- On line 202 "calibration" should be "calibrate"

- On line 213 "tripe" should be "triple"

- On line 288, "an" is missing before "elastic"

- On line 476, the sentence should begin "It satisfies the condition that…"

- On line 486, I suggest revising to "The incoherent synthesis more accurately represents our experimental implementation..."

- The sentences between lines 512-516 need to be proofread for language usage and corrected

(Remarks on code availability)

Referee #2

(Remarks to the Author)
The authors have done a very good job revising the manuscript and clearing up the remaining questions. As stated originally, this paper is an important advancement in the field of Volumetric Additive Manufacturing which merits publication in Nature. The reviewer recommends acceptance for publication at this point. There are a few more points which would be of interest but none of them merit further delay of publication at this point. Very well done!

(Remarks on code availability)
The code is well documented and the logic is clear.

Response to Reviewers –

We sincerely thank the reviewers and editors for their insightful comments and constructive feedback on our manuscript entitled "Sub-second Volumetric Additive Manufacturing by Digital Incoherent Synthesis of Holographic Light Fields." We have thoroughly revised the manuscript in response to all concerns and provide below a detailed, point-by-point response. Additions and major changes in the revised manuscript are indicated by highlighting in red. For ease of communication, the original referee comments are shown in black color, whereas our specific answers are in blue. Thank you again for your great efforts.

Referee #1

The manuscript by Xukang Wang and coworkers reports an important accomplishment in the field of volumetric 3D printing. The authors are to be congratulated and commended on their impressive demonstration of sub-second volumetric printing, the capability to print through a flat interface deep into a volume (rather than requiring 360 deg of optical access around a cylindrical perimeter), the meticulous and careful characterization and calibration of their optical system, and its demonstration with multiple materials and flow-coupled fabrication. These technical achievements are a significant advance in the field of volumetric photopolymer 3D printing (and beyond), and will surely be noted by the community. The experiments are carefully executed, the manuscript is mostly well-written and well-organized, and the results are mostly presented in appropriate detail.
However, for publication in a high-impact journal with an extremely broad readership such as Nature, revisions are necessary to more clearly describe the key principles that allow for these achievements, and place the work more completely into the relevant context. I would recommend acceptance of the manuscript after significant revisions that address the following questions and provide additional details as follows.

Response:

We greatly appreciate the reviewer's positive assessment of DISH, especially on the printing speed and flat-interface volumetric printing. We have added data and a discussion section in response to the constructive comments on the resolution and holographic algorithm. We summarized the revisions corresponding to the reviewer's comments as follows:

- We corrected the dimensions to mJ/cm^3 for dose and updated the relevant equations and descriptions.
- We clarified how our holographic algorithm works and its rationale, and discussed the efficiency of the algorithm. Also, the necessity of coherent light source and the influence of speckles were shown.
- New results and discussion were added to better clarify the experimental accuracy/resolution. We have added new printing results to indicate that the overall resolution is about 19 μm and the finest positive feature is measured as about 12 μm. Dimensional accuracy test by CT scanning was also quantified and added.
- We explained why binarization must be conducted within each optimization loop.
- Details regarding the voxels and throughput were updated according to the comments, and we specified the voxel size as well as the printing volume.
- Viscosity data were added (Supplementary table 1). The figure for mass production was updated (Fig.5c); labels, units, fonts, and other details of the figures were revised; contents about 3D display were removed as suggested.

OPTIMIZATION OF ABSORBED DOSE

The authors optimize the light fields based on calculating accumulated dose (lines 135-140), and its difference with a high and low threshold. They define "dose" as the product of intensity I(x→) and exposure time Δt. Later, the equation on lines 392 and 404, and associated discussion similarly refer to this type of "dose" calculation. This is incorrect – the product of time and intensity is (areal) radiant exposure (units of mJ/cm^2), appropriate to use in a layer-by-layer printing context, when light is impinging onto a flat layer of resin. When calculating doses in a volumetric context, a volumetric absorption factor must also be included (units of 1/cm), which is derived from the resin absorbance. I would recommend reviewing the supplements of Tumbleston et al [ref 13 of this manuscript] or following the approach of references [17] or [18] for calculations of volumetric absorbed dose. Refer also to Pritchard et al https://doi.org/10.1002/admt.201900700 where volumetric dose estimation is appropriately reported with layered printing as well. This fundamental misconception must be corrected, so that dose can be calculated/optimized in appropriate physical units of mJ/cm^3.

Response:

We highly appreciate the reviewer for pointing out the misconception of dimensions. The laser intensity is expressed in units of mW/cm^2, and when multiplied by time, it yields unit of mJ/cm^2. In contrast, the unit of average absorbed energy per volume should be mJ/cm^3 in volumetric printing.

To correct this, we extract the absorption factor μ out of the propagation matrix

$\mathcal{H}_\varphi$, and revise the accumulated dose from $I(\vec{x})\Delta t$ to $\mu(\vec{x})I(\vec{x})\Delta t$. The absorption factor is denoted as $\mu(\vec{x})$ because beams from all projection angles φ share the same propagation distance for a given position $\vec{x}$.

The revised loss function is

$$L = \sum_{\vec{x}\in A} |d_h - \mu(\vec{x})I(\vec{x})\Delta t|^2 + \sum_{\vec{x}\in \tilde{A}} |\mu(\vec{x})I(\vec{x})\Delta t - d_l|^2$$

The revised propagation matrix is

$$\mathcal{H}_\varphi(z_\mathrm{r}) = \mathcal{F}^{-1} H(z_\mathrm{r} + l_\mathrm{r}, \lambda_\mathrm{r}) \cdot S_\varphi \cdot H(l_\mathrm{i}, \lambda_\mathrm{i})\mathcal{F}$$

Correspondingly, the equations and descriptions in the article are revised as listed below.

(1) revised line 138

$$\begin{cases} \min \quad L = \sum_{\vec{x}\in A} |d_h - \mu(\vec{x})I(\vec{x})\Delta t|^2 + \sum_{\vec{x}\in \tilde{A}} |\mu(\vec{x})I(\vec{x})\Delta t - d_l|^2 \\ \mathrm{s.t.} \quad I = \sum_\varphi \left|\mathcal{H}_\varphi\left(\delta_\varphi u\right)\right|^2, \quad \delta_\varphi \in \{0,1\} \end{cases},$$

where $\vec{x}$ represents the 3D coordinates in the objective area, φ represents the projection angle, $\mu(\vec{x})$ represents the absorption during the propagation in materials, and thus $\mu(\vec{x})I(\vec{x})\Delta t$ represents the accumulated dose at each point. A represents the 3D region of the target model to be printed, where the accumulated dose is expected to be d_h for polymerization; and $\tilde{A}$ represents the area outside the target region where the accumulated dose is supposed to be smaller than the threshold d_l to avoid overexposure.

(2) revised line 453

$$\begin{cases} \min \quad L = \sum_{\vec{x}\in A} |d_h - \mu(\vec{x})I(\vec{x})\Delta t|^2 + \sum_{\vec{x}\in \tilde{A}} |\mu(\vec{x})I(\vec{x})\Delta t - d_l|^2 \\ \mathrm{s.t.} \quad I = \sum_\varphi I_\varphi^{\mathrm{coarse}} \end{cases}$$

The descriptions are changed accordingly, similar to the above-mentioned one.

(3) revised line 467

$$\begin{cases} \min \quad L = \sum_{\vec{x}\in A} |d_h - \mu(\vec{x})I(\vec{x})\Delta t|^2 + \sum_{\vec{x}\in \tilde{A}} |\mu(\vec{x})I(\vec{x})\Delta t - d_l|^2 \\ \mathrm{s.t.} \quad I = \sum_{\varphi' \notin \{\varphi g\}} I_{\varphi'}^{\mathrm{temp}} + \sum_{\varphi g} \left|\mathcal{H}_{\varphi g}\left(\delta_{\varphi g} u\right)\right|^2, \quad \delta_{\varphi g} \in \{0,1\}, \qquad g \in \{1,2,\dots,G\} \end{cases}$$

UNCLEAR HOW AND WHY HOLOGRAPHIC LIGHT FIELDS ENABLE THE REPORTED RESULTS:

The authors emphasize the importance of their use of a coherent laser source, and the use of holographic light fields to expose the resin. The conventional understanding of holographic light projection involves the shaping/control of both the amplitude and phase of the light. Yet, the pattern generating device used here is a DLP9500 (manuscript line 303), which controls only amplitude, and the authors' only mention of optical phase is on line 414-415, to say that the "phase is constant" in their optimization. The authors model light propagation using complex fields in a wave-optics approach (lines 127-147, and 327-349), and this appears to be a correct and fully-holographic description of the system (note also the recent paper from Wechsler et al reporting a wave-optical mode https://doi.org/10.1364/OE.521322 which should be cited). However, if their hardware is not applying any phase-shaping to the optical pattern, and the phase profile of the source laser is not being measured or controlled, and the phase is a constant in the complex propagation optimization, why is holographic (complex amplitude) necessary at all? Why must the holographic light fields be incoherently synthesized (i.e. their intensities superimposed, but phase interference is not part of the picture)? This needs to be more clearly explained. The trade-off for this approach is computational expense, with the algorithm taking 24 hours to complete (line 427). Is the trade-off worth the gain in accuracy? The authors do not discuss this.

Response:

We appreciate the reviewer's insightful comments on the usage of holography and its results. Here, we use holographic light field to emphasize the necessity of coherent light source for extended depth of field and the necessity of modeling complex field during optimization. We do not use complex field modulation devices in our system but we are able to introduce the modulation of complex field across the 3D volume via DMD binary intensity modulation.

Incoherent synthesis of holographic light fields is not our design target; this method is instead tailored to our experimental implementation, as the projected beams at different moments are mutually incoherent in our system. Our results show that it's sufficient to use incoherent synthesis of the coherent light field to generate high-precision 3D patterns. Coherent synthesis of coherent light fields may represent another viable approach to explore in the future.

With respect to the algorithm computational cost, our voxel computational efficiency has been higher than that reported in the wave optical mode VAM study (reference has been added as [25]) for the same number of voxels. Future work may utilize deep neural networks to further reduce the computational costs.

The detailed responses to the reviewer's comments, along with the corresponding revisions made to the manuscript, are provided below.

(1) Phase update:

The phrase "phase is constant" in the paper is a mathematical assumption only within the current iteration to simplify the process of differentiating complex numbers. This assumption is necessary because complex functions like $|u|^2$ are non-analytic and their precise derivative forms are difficult to calculate ($\mathrm{d}|u|^2 = u\mathrm{d}\bar{u} + \bar{u}du$, where $\bar{u}$ is the complex conjugate), but their approximated forms are quite easy under the constant phase assumption ($\mathrm{d}|u|^2 \approx 2\phi^{-2}(u) \cdot udu$, where $\phi(u)$ is the assumed constant phase factor of u). Throughout the entire optimization process, the three-dimensional phase is not constant and changes as the DMD patterns are updated.

The retrieval of the phase information is a key point in computational holography. Specifically, the phase information plays a crucial role in the accurate calculation and control of intensity beyond the depth of field, as well as in characterizing aberrations induced by refraction.

The phase in 3D volumes can be modulated by DMD patterns. The DMD itself is not a phase-modulating device; however, when beam propagation is considered, beams interfere within the printing region, resulting in changes to both amplitude and phase. To illustrate this simply, Fig. R1 presents the complex amplitudes projected by two patterns (before and after optimization), with phase represented by color. Notably, when a pattern includes high-frequency spatial components, the phase exhibits drastic spatial variations.

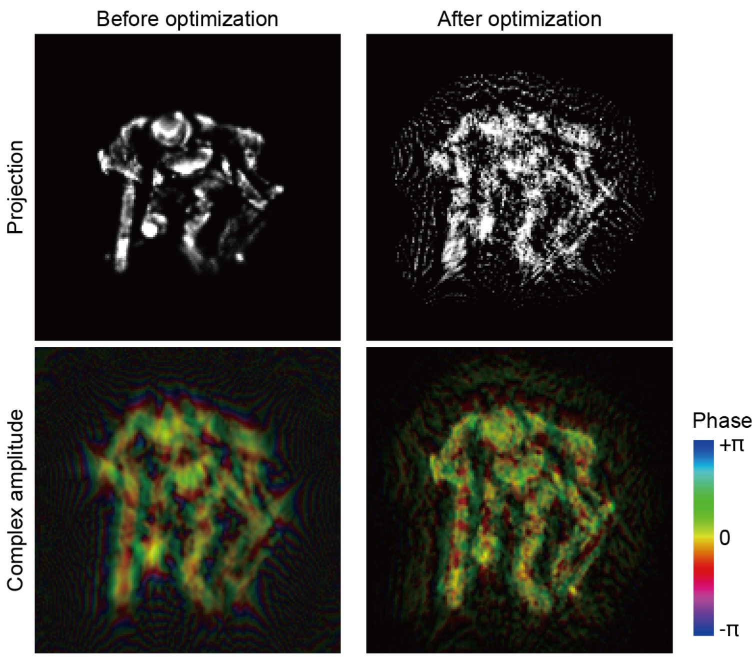

Figure R1: Simulated amplitude and phase distributions projected by the DMD patterns before and after optimization. For the complex amplitude, the amplitude is represented by brightness, and the phase is represented by color. After optimization, not only do the edges of the amplitude distribution become sharper, but the phase also exhibits more pronounced spatial variations. This indicates that the amplitude-only DMD patterns can effectively influence both the phase and amplitude of the projected complex amplitude.

The revised paragraphs include: “Within each iteration, the phase of $\mathcal{H}_\varphi V_\varphi$ is assumed to be constant, and the binarization error is temporarily ignored, that is $\left|\mathcal{H}_\varphi V_\varphi\right|^2 \approx \sum_{\varphi g}\left|\mathcal{H}_{\varphi g}\left(\delta_{\varphi g} u\right)\right|^2/G$, thus the gradient descent of V_φ can be approximated.” (line 476).

(2) incoherent synthesis

The incoherent synthesis refers to the superposition of beams projected at different moments, which includes both the superposition of 180 angles in the coarse step and the superposition of 10 binary projections in the fine step. The sequenced projection makes the beams of different moments incoherent to each other, and therefore, incoherent synthesis better describes the actual physical process in our experimental setup. In contrast, coherent synthesis is not adapted in our work for its complete different experimental design.

Coherent synthesis means that the beams from different angles are coherent to each other. A typical application is three-dimensional holographic lithography, where the projected beams interfere to produce three-dimensional photonic crystals with periods comparable to the wavelength (https://www.nature.com/articles/35003523). In the future, system designs for arbitrary 3D shape printing via the coherent synthesis of coherent light fields may emerge.

The revised paragraphs include: “The incoherent synthesis is more compatible with our experimental implementation, thereby reducing dose estimation errors.” (line 486)

(3) Computational cost

While current 3D holographic algorithms are inherently time-consuming, our approach exhibits competitive efficiency relative to existing methods. In the paper “Wave optical model for tomographic volumetric additive manufacturing” (reference added as [25]), processing 550×550×550 voxels across 600 angles took 4 hours on an NVIDIA A100 with 80GB GPU RAM. In contrast, our algorithm processes a 1350×1350×1852 voxel volume across 1800 angles in 24 hours without GPU acceleration. Notably, our voxel count is 20-fold higher than that of the aforementioned method, yet our runtime is only 6-fold longer, demonstrating that our algorithm requires less time for an equivalent voxel volume.

Although our method has been shown to achieve superior resolution, we acknowledge that its computational cost remains prohibitive for practical applications. Future efforts will focus on advancing such techniques for better computing efficiency. Beyond GPU implementation, we hypothesize that holographic algorithm efficiency can be substantially enhanced via neural network integration. For instance, the end-to-end neural network approach presented in *End-to-end learning of 3D phase-only holograms for holographic display* accelerates 3D hologram generation to 5 frames per second. In the meantime, the utilization of deep learning may arouse another problem of generalization and fidelity. Therefore, we use conventional optimization algorithm here and have cited related works, indicating the potential of deep learning to reduce the computational costs in future works.

The revised paragraphs include: "As for the computational cost of the algorithm before the printing process, DISH is comparable to other computed holographic methods[25]. Still, after acquiring high-resolution datasets that account for refractive aberrations, introducing end-to-end neural networks for 3D hologram generation[40,41] and GPU acceleration may further reduce the computational cost." (line 314)

Additionally, Fig 1d and lines 119-124 emphasize the benefit of a coherent source, but the authors do not quantify the coherence of their laser. Please provide either the spectral bandwidth or the coherence length of the laser. Lastly, coherent sources inevitably carry with them the drawback of speckle noise, which can significantly degrade printing accuracy, and which must usually be countered by a variety of means. No such noise is discussed or mitigation shown in this manuscript, which is an omission that must be corrected.

Response:

We sincerely apologize for the inadequate explanation regarding laser coherence and speckles. The linewidth of the laser used in our experiments is 1.5 nm.

In our system, speckles arise from inherent imperfections of the laser, dust and scratches in the optical path, and hologram artifacts. The intensity inhomogeneity induced by speckles does introduce streak-like artifacts on the sample surface, such as the tilted textures depicted in revised Fig. 4a-c.

Notably, the impact of speckles on our system is less pronounced than their effect on samples in traditional perpendicular-projection setups. In traditional volumetric printing (as reported in https://arxiv.org/pdf/2506.02578), samples tend to develop horizontal stripes. This is because speckle-induced textures are consistent with the beam propagation directions, while all beam directions are perpendicular to the rotation axis in conventional designs. The superposition of these textures leads to an increase in inhomogeneous contrast. In our system, by contrast, beams are projected at inclined angles; the resulting textures do not fully overlap, which yields a relatively lower dose inhomogeneity contrast. As shown in Fig. R2, the speckle-induced textures on our printed samples are comparable to those of traditional volumetric printing systems equipped with speckle noise reduction technology.

[redacted]

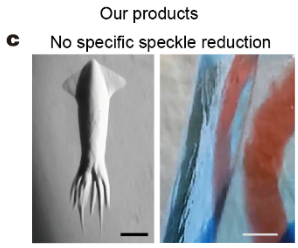

Figure R2: Comparison of speckle impact on samples printed by conventional and our volumetric printing systems. [redacted] **c,** Samples printed by our methods, without specific speckle reduction, exhibit tilted stripes. The speckle-induced textures in (a–c) are all consistent with the beam projection direction of their respective system. Our system employs multiple obliquely projected beams, leading to minimal overlap between the resulting speckle-induced textures. Consequently, the speckle-induced textures on our printed sample (c) are comparable to those on the speckle-noise-reduced samples in (b). Scale bar: 500 µm.

Nevertheless, the issue of laser speckles remains to be addressed. Potential solutions include the following: (1) Integrating devices such as galvanometers to enable additional rapid translation or rotation of the light beam, thereby reducing the contrast of speckles. (2) Advancing holographic algorithms, such as using multiple holograms or tiled holograms to reduce speckle noise. We have supplemented the relevant content in the discussion section in line 331:

"Another factor reducing product quality is speckle noise, which causes intensity inhomogeneities and stripe-like artifacts along the light propagation direction. The traditional perpendicular projection causes stripes to overlap, forming transverse patterns. In contrast, our inclined projection system avoids this issue, resulting in less prominent stripes. Nonetheless, the surface quality could be further improved by using multiple or tiled holograms to suppress speckle noise, or introducing beam translation or small deflections via optical components."

THE TRUE ACCURACY/RESOLUTION OF THIS TECHNIQUE IS UNCLEAR

The highest-resolution prints, which are used to demonstrate the 11 µm resolution (Fig 3g and 3h, as well as Figure S11) are only shown as ridges/lines on a much larger bulk slab. Can the authors explain why, for instance, they do not show free-standing structures or other features of similar size? All prints besides these figures show much larger and coarser features, with less-accurate results. The structures in Fig 4 seem to have surface waviness or distortion on a scale of ~100 µm at best (see below). It may be the case that the achievable *optical* resolution of this system reaches 11 µm, and can only reproduce features at that size when textured onto larger objects. But when reaction-diffusion tradeoffs due to the photochemical kinetics come into play, such fine features do not seem to be attainable. This does not invalidate the authors' results, but must be discussed, and cannot be swept under the rug. (Note that similarly, the optical system in Toombs et al (Ref 21) is reported to have a modulation transfer function of ~100 cycles/mm, which would yield a resolution of 5-10 µm, but the structures can only be fabricated with ligaments/elements down to about 50 µm in width).

Response:

We thank the reviewer for pointing out this ambiguity. The true printing accuracy/resolution is really an important part of 3D printing techniques, and we add new results and discussions to clarify this part according to your suggestion.

To provide a more compelling demonstration of the printing ability, we have added three new models. First, the fishbone model with designed rib widths of 2 pixels (10.8µm) was printed to show the finest resolution of positive features. The printed product is shown below in Fig. R3 (revised Fig. 4h-i), the experimental width after printing is measured as 11.9±2.1 µm, close to the optical resolution and textured resolution. Further, for more complex 3D models, a conch model was printed, with lines in different directions and z-axis positions. The lines after printing are measured as 19.3±3.4 µm (Fig. R4 and revised Fig. 4l-o). There are jagged edges on the line structures, which are mainly due to the pixel aliasing error caused by the 5.4-µm pixel size used in the modeling process. In summary, the overall resolution of our printing for diverse structures is about 19 µm. For positive feature tests, we can achieve minimum structure of 12 µm. Therefore, the descriptions about the printing resolution have been revised to 19 µm in the abstract, introduction, and updated results to prevent misunderstanding.

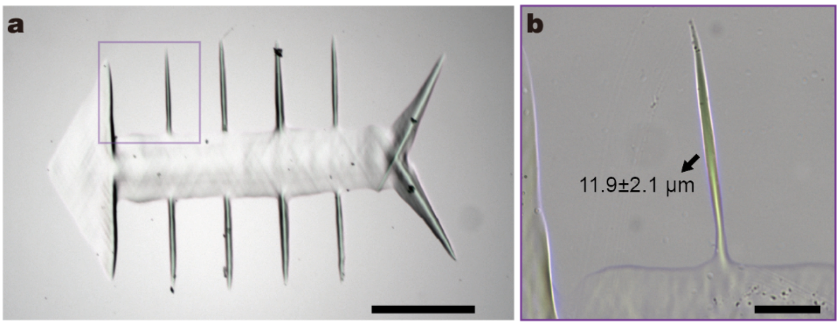

Figure R3: Fishbone model for the positive feature test (Fig. 4h-i). a, Printed fishbone model with designed rib widths of 10.8 μm. **b,** Close-up view of (a). The measured rib width is 11.9±2.1 μm, representing the finest printable positive features of DISH. Scale bar: 500 μm (a) and 100 μm (b).

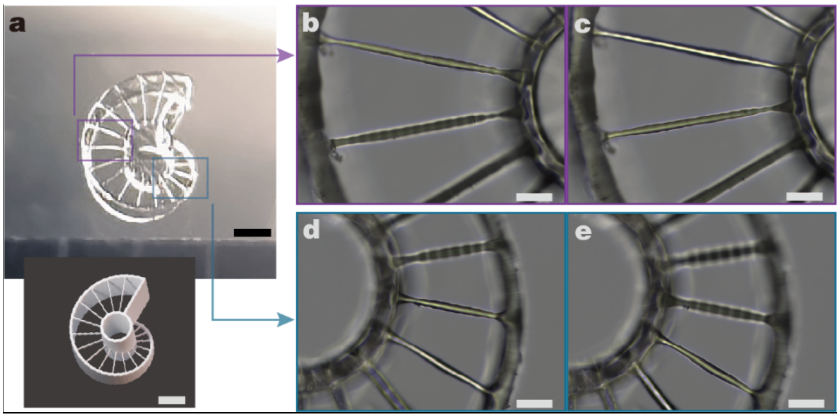

Figure R4: Conch model for comprehensive resolution test. (Fig. 4l-o) a-b, Conch model and its printout. Lines are arranged along different directions and z-axis positions. **c-f,** Close-up views of distinct lines. As the lines are distributed across z-axis positions, those outside the microscope's focal plane appear as defocused patterns. The measured width of these lines is 19.3 ± 3.4 μm. This model enables the characterization of the stable resolution achievable by DISH at various positions when printing more complex structures. Scale bar: 500 μm (a-b) and 100 μm (c-f).

We think that the surface waviness of distortion on a scale of ~100 μm may be the undersigned surface textures caused by speckles. We have supplemented the potential solutions to reduce the speckles in the discussion section in line 331: "Another factor reducing product quality is speckle noise, which causes intensity inhomogeneities and stripe-like artifacts along the light propagation direction. The traditional perpendicular projection causes stripes to overlap, forming transverse patterns. In contrast, our inclined projection system avoids this issue, resulting in less prominent stripes. Nonetheless, the surface quality could be further improved by using multiple or tiled holograms to suppress speckle noise, or introducing beam translation or small deflections via optical components."

ADDITIONAL IMPORTANT, BUT LESS FUNDAMENTAL ISSUES TO CONSIDER:

1. The dimensional accuracy of most of the printed structures is difficult to assess (e.g. all structures in Fig. 4). Please compare at least once or two final printed structures (not only the modeled dose distributions in Fig 2d and S6, S7) to the original source geometry. A CT scan or laser-based surface scan of a print can provide this information (refer to Ref 25 or Ref 22, or the more recent report from the same group https://doi.org/10.1016/j.addma.2024.104480). {Note, relatedly: please add units to the y-axis of the signed distance plots in Supp Figures 6 and 7}.

Response:

We sincerely appreciate the reviewer's constructive suggestion. We reprinted the model of Theodoric and performed a CT scan using Zeiss Xradia 620 Versa, as shown in Fig. R5 (revised Fig. S10h). However, for unsupported structures, deformation during post-processing is hard to totally avoid. For example, the shift at the end of the left stick causes extra mismatch between the products and the model. The root mean square (RMS) of the signed distance for the CT scan model is 45.7 μm. The units of the y-axis of the signed distance plots in Supplementary Figures 6 and 7 have been added.

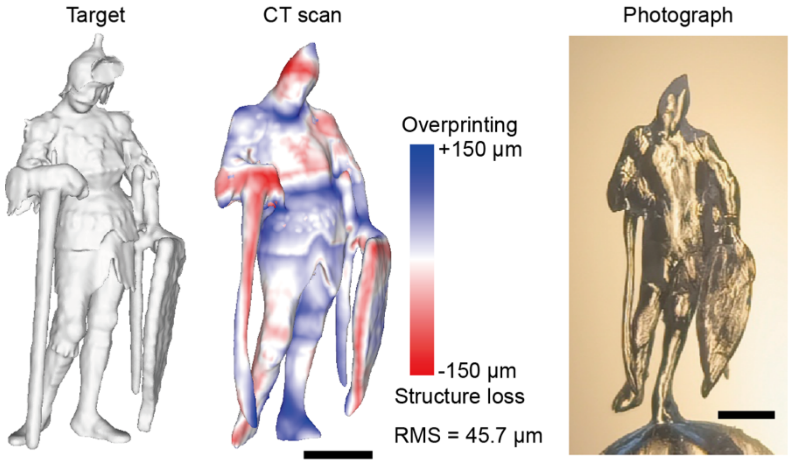

Figure R5: CT scan of the Theodoric sample (Fig S10h). The target model, the model reconstructed by CT scanning of the printed sample, and the image of the sample are demonstrated. The signed distances relative to the target model are visualized by color. Deformation of unsupported structures during post-processing led to additional accuracy loss. The final RMS of the signed distance is measured to be 45.7 μm. Scale bar: 1 mm.

2. The discussion of binarization is extremely confusing. It seems that this is a way of

overcoming the native pulse-width-modulated (PWM) method that the DMD typically uses to generate grayscale images. The authors instead seem to be generating binary image-sets at various bit-depths to encode the grayscale intensity maps calculated by the algorithm. Why this must be done *inside* the optimization loop and then projected using the wave-optics operators is not clear, nor how this improves the results of the optimization. For instance, why not run the optimization loop on the complex-valued field, and only run binarization after the optimization completes?

Response:

Thanks for the reviewer's insightful inquiry. There's a significant discrepancy between the intensities projected by a grayscale pattern and its corresponding binarized pattern sequence. As illustrated in Fig. R6, the intensity contrast decreases remarkably after binarization. A primary reason for this is that beams projected at different time points undergo incoherent synthesis. Thus, compared to the original grayscale pattern, the time-induced loss of coherence results in reduced light intensity contrast.

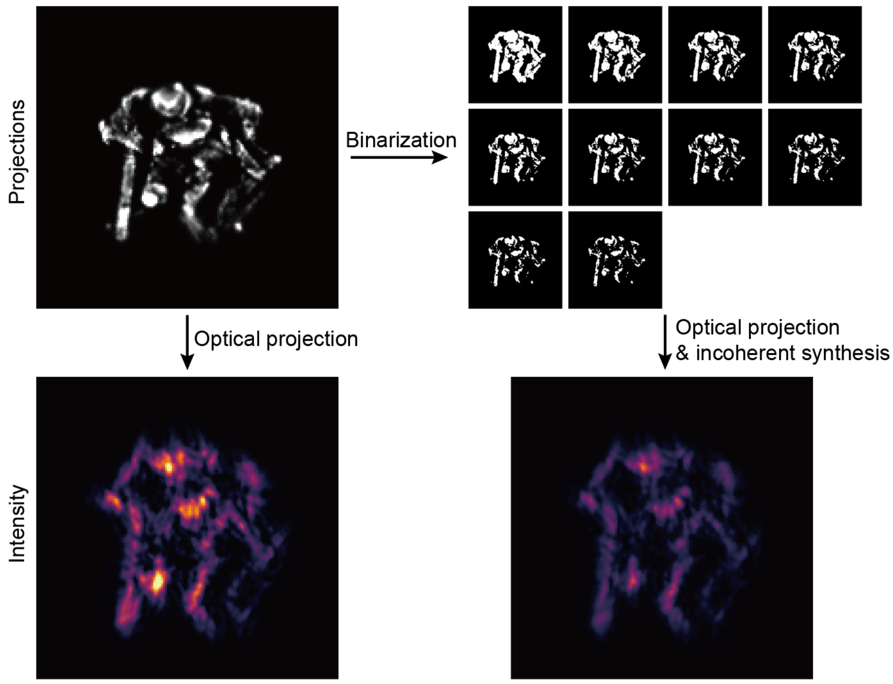

Figure R6: Binarization error of the projected intensity. Intensity obtained via direct optical projection is compared with that obtained via binarization followed by incoherent synthesis. Direct optical projection yields an intensity distribution with a shape similar to that of incoherent synthesis but markedly different contrast. Since incoherent synthesis better aligns with the actual physical process of the employed DMD, intensity information derived from direct optical projection leads to errors in dose estimation and is thus unsuitable as a reference for dose optimization. Incorporating the binarization process into the loop can minimize this binarization error.

Volumetric printing is highly sensitive to dose contrast, so such errors introduced by binarization must be avoided. Therefore, binarization should not be treated as the final step of the algorithm. Performing binarization within the loop allows for a more accurate dose distribution simulation, facilitating the iterative algorithm.

Our current binarization method is specifically tailored to the projection characteristics of the DMD. While the DMD's modulation capability is limited to binary modulation, its speed advantage with a refresh rate exceeding 18 kHz allows diverse modulation of complicated patterns. We have added more discussions in the revised manuscript to illustrate the binarization process.

The revised paragraphs include: "The binarization process must be performed within the loop because of the binarization errors, that is, the intensity of direct projection $\left|\mathcal{H}_{\varphi} V_{\varphi}\right|^2$ differs from that of the incoherent synthesis of binary projections $\sum_{\varphi g}\left|\mathcal{H}_{\varphi g}\left(\delta_{\varphi g} u\right)\right|^2 / G$. The incoherent synthesis is more compatible with our experimental implementation, thereby reducing dose estimation errors." (line 483)

3. The authors claim "low viscosity" on lines 34 and 110 but the viscosities are not reported. Please measure and report viscosities of the various resins. Viscosity is a critical parameter in volumetric 3D printing and it is important for comparison with other investigations in the field.

Response:

We appreciate the suggestions about viscosity. The viscosity of each material used in this work has been measured as below and added as supplementary table 1:

Material	**Viscosity (cP)**
20% PEGDA hydrogel	4.734
20% SilMA hydrogel	40.12
10% GelMA hydrogel	14.15
PEGDA mixed solvent	63.85
PEGDA resin	99.11
BPAGDA resin	656.38
DPHA resin	750.49
UDMA resin	562.99

Table R1(Supplementary Table 1): Viscosity of experimental materials.

The viscosities of materials used in VAM are usually between 6000~10000 cP, while all of the materials we use are less than 1000 cP due to the high printing speed. Generally, materials with a viscosity of less than 100 cP are frequently used and demonstrated.

4. In the Abstract, the authors mention “a tradeoff between precision and efficiency” (line 26) implying that this work moves beyond that trade-off (a better way to describe the trade-off is between resolution and volumetric build rate). This is not quite convincingly demonstrated. Supplementary Figure 1 is meant to illustrate this, and manuscript lines 273-276 mention some metrics about throughput. Why is the addressable volume only 200 mm^3 when line 426 later says that the addressable volume is 7.3x7.3x10 mm = 533 mm^3? And the voxel size given on line 275 indicates that the voxels of this approach are rhomboidal (not parallelepipedal). This needs to be discussed further, to support the claim of going beyond the resolution/build rate trade-off. Supplementary Figure 1 would be more informative and convincing if the axes were switched (minimum feature size on the x-axis, throughput on the y-axis) and the “scanning and exposure time” metric were converted to volumetric build rate (mm3/s), similarly to figures from Hahn et al https://doi.org/10.1002/adfm.201907795 and https://3dprintingspeed.com or Wirth et al https://doi.org/10.1016/j.addma.2024.104081

Response:

We sincerely appreciate the reviewer’s comments regarding the efficiency and resolution. We have altered the wording in the abstract as recommended (the tradeoff between resolution and volumetric build rate) and revised the discussion part in line 299 as follows to make the statement clearer:

“In additive manufacturing, higher spatial resolution or smaller voxel size results in a significant increase in the number of voxels required per unit volume, which consequently decreases volumetric build rate. Conversely, enhancing volumetric build rate often occurs at the cost of reduced resolution. Voxel printing rate is therefore a parameter that enables intuitive characterization of 3D printing efficiency across multiple length scales. Using DISH, a sample with a volume of approximately 200 mm^3 (Supplementary Fig. 3c) can be produced in a minimum exposure time of 0.6 seconds, achieving a volume printing rate of 333 mm^3/s and a voxel printing rate of 1.25×10^8 voxels/s at a voxel size of $(11\ \mu m)^2\times22\ \mu m$ (Supplementary Fig. 9e). Compared with other 3D printing methods, DISH shows great improvement in speed and resolution when manufacturing millimeter-scale samples (Supplementary Fig. 1).”

To better compare efficiency with other methods, we have adjusted the vertical axis of Supplementary Figure 1 to mm^3/s, and the new figure is shown as Fig. R7:

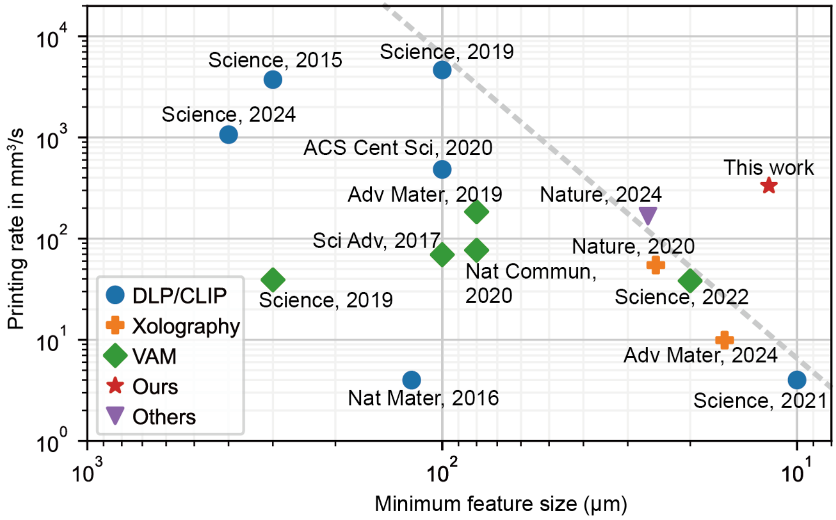

Figure R7: Benchmarking of DISH and state-of-the-art 3D printing methods. (**Fig. S1**) The gray dashed line in the figure represents a voxel efficiency of approximately 6.5×10^6 voxels/s, estimated under the assumption that the voxels in these works are cubes with side lengths equal to the minimum feature size. Our system achieves a voxel efficiency of 1.25×10^8 voxels/s, exhibiting advantages among printing methods of the same scale.

Regarding the printing volume, 200 mm^3 is calculated based on the volume that can be irradiated by beams from all angles. As shown in Fig. R8, when the DMD always projects a circular pattern, the printing area is a centrally symmetric spindle shape, which can be approximated by a cylinder and two cones. The volume of the cylinder is $\pi\left(\frac{d}{2}\right)^2\cdot\frac{d}{\tan\theta_r}\left(\frac{1}{\cos\theta_i}-1\right)$, and the volume of two cones is $2\cdot\frac{1}{3}\pi\left(\frac{d}{2}\right)^2\cdot\left(\frac{d}{2\tan\theta_r}\right)$. The total volume is thus $\frac{1}{4}\pi d^3\frac{1}{\tan\theta_r}\left(\frac{1}{\cos\theta_i}-\frac{2}{3}\right)$, where d is the beam diameter, θ_i is the incident angle, and θ_r is the refracted angle. The short side length of the DMD is 1080 × 10.8 μm = 11.664 mm, and after 2-time beam reduction, the beam diameter is d=5.832 mm. When the refractive index of the material is 1.48, the refraction angle θ_r≈28.54°, and the volume is about 214.1 mm^3. Since the shape is not a strict combination of a cylinder and cones, and the spindle vertices are often unused, we estimate the printing region to be 200 mm^3. Additionally, because the shape of DMD is rectangular and the periscope design allows a maximum beam diameter of 6 mm to pass through, the final printing area will include some additional irregularly shaped areas. Larger printing area can be obtained with a DMD projector with a larger pixel number without reducing the printing speed.

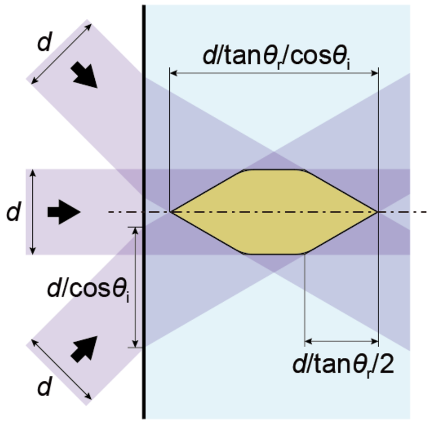

Figure R8: Shape of the printing area (Fig S3c). The printing area of the system is defined as the region illuminated by light beams from all angles. When the light beam has a circular cross-section with diameter *d*, the printing area approximates a spindle-like structure. When its volume is approximated using a cylinder and two cones, the volume can be expressed as $\frac{1}{4}\pi d^3 \frac{1}{\tan\theta_r}\left(\frac{1}{\cos\theta_i}-\frac{2}{3}\right)$, where θ_i denotes the incident angle and θ_r denotes the refracted angle. When *d*=5.832 mm (the short-side width of the DMD is reduced by a 2× beam reducer)， the material refractive index is 1.48, and the incident angle is 45°, the approximated volume is calculated to be 214.1 mm^3.

The model size is set as 7.3×7.3×10.0 mm^3 in algorithms, which is larger than the bounding box of the printing area. This is because, in our system, areas surrounding the printing area may also cure due to excessive dose, which must be considered in the algorithm.

Regarding the voxel size, the voxel size is determined by capturing the photographs of densely arranged points projected in a coumarin-30 DMSO solution. As shown in Fig. R9 (Fig. S9e), the shape of a projected point is close to a cylinder, and its circumscribed cuboid is defined as the voxel.

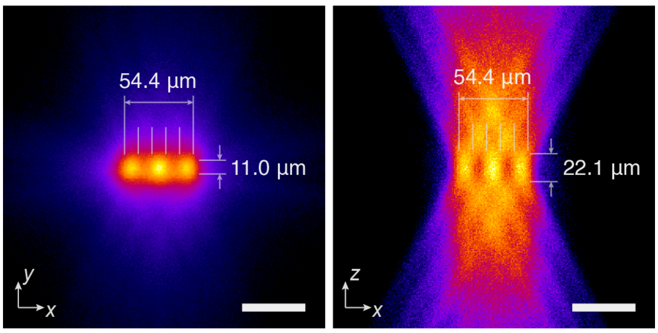

Figure R9: Experimental measurement of the voxel (Fig. S9e). Our voxel is defined as the bounding cuboid of the smallest clearly distinguishable projected point. A dense dot array pattern was projected into a coumarin-30 fluorescent solution, and their 3D dimensions were measured to be $(11.0\ \mu m)^2 \times 22.1\ \mu m$. Scale bar: 50 μm.

REQUESTED MINOR CHANGES:

-- The abstract claims "massive [sic] continuous flexible production" (what is meant, I think, is mass fabrication or mass production). However, Supplementary Video 2 makes clear that structures are produced in a stop-flow mode, at a rate of ~0.2 Hz. This is a fine approach, but to describe this as "continuous" is inaccurate. Can the authors comment on a maximum possible rate? Although Figure 4c shows a handful of structures, this is not yet at "mass fabrication" throughput; being able to show e.g. 10s or 100s of objects would be preferable before claiming mass fabrication.

Response:

We appreciate your valuable suggestions regarding continuous and mass production. "Stop-flow" is indeed more accurate for our system design. We have revised the relevant text accordingly:

1. In the abstract, "massive" is replaced by "efficient" (line 26) or "mass" (line 35) and the word "continuous" is deleted in relevant paragraphs.

2. In the introduction, line 46 is revised as "Efforts have been made to enhance the production rate". Line 49, we add the word *batch production* to describe the "roll-to-roll" printing, for it prints a batch of products on the conveyor, and then the conveyor moves for the next batch of printing. Line 64 is revised as "restricting its possibility of integrating flow control to further improve the printing efficiency". Line 70, "continuous fabrication" is adapted to "successive fabrication" and so is line 91.

3. In the results, figures, and discussion (previously conclusion) part, the word "continuous" is replaced by "successive" when generally referring to a fabrication mode. Regarding the fluidic system, our current experimental setup merely fulfills basic functionality, leaving substantial room for future improvement. We identify fluid control as the primary factor limiting the speed of successive printing: first, low-viscosity materials must rapidly transition from a flowing to a stationary state to mitigate convection during exposure; second, post-exposure flow must be uniform to minimize disruption to the newly printed structure.

In practice, we have implemented a relatively conservative interval to avoid such disruptions; theoretically, with an ideal fluid control system that eliminates the aforementioned limiting factors, the printing speed could approach 1.6 Hz (corresponding to a 0.6 s exposure time).

Furthermore, we have added the results with 10s of objects to show our capability of mass production as suggested by the reviewer, as shown in Fig. R10 (revised Fig. 5c).

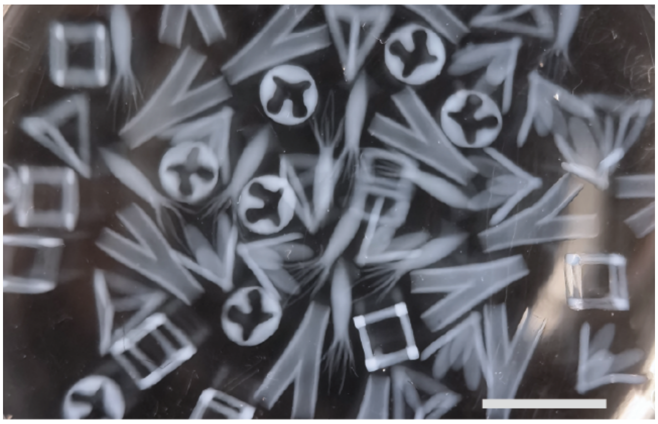

Figure R10: Diverse structures printed at high speed by DISH (Fig. 5c). More products obtained via successive printing are demonstrated, highlighting our mass production capability. Scale bar: 5 mm.

-- In Fig 3g (and in Supplementary Fig 11), please indicate by overlay or arrows which were the relevant stripe patterns and what their designed dimensions are (compared to the measured 54, 11, 15.5, 20.9 and 33.1 μm line widths).

Response:

We appreciate your valuable suggestions regarding original Fig. 3g (revised Fig. 4a) and Supplementary Fig. 11 (revised Fig. S10a). The designed line widths of each group are 10, 2, 3, 4, and 6 pixels, respectively. They correspond to 54.0, 10.8, 16.2, 21.6, and 32.4 μm. The labels have been added to the figures.

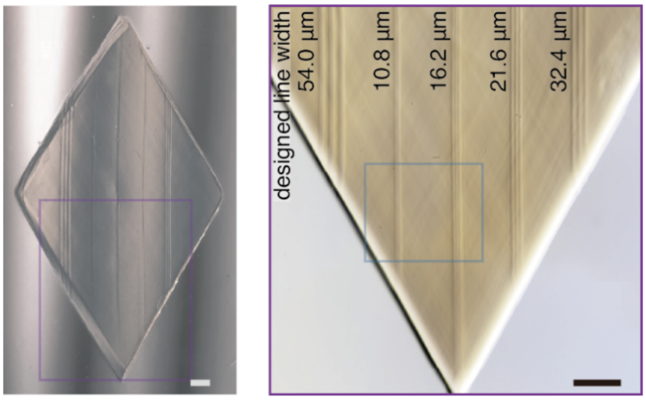

Figure R11: Samples demonstrating the smallest feature size. (revised Fig. 4a). The designed widths have been added. The line widths were designed as 54.0, 10.8, 16.2, 21.6, and 32.4 μm, while the line widths were measured as 54.0±2.9, 11.0±1.2, 15.5±1.9, 20.9±2.3, and 33.1±2.1 μm, respectively. Scale bar: 500 μm.

-- Please add units for signed distance calculations of Supplementary Figures 6 and 7.

Response:

We thank the reviewer for careful suggestions regarding Supplementary Figs. 6 and 7. The units have been added and shown below.

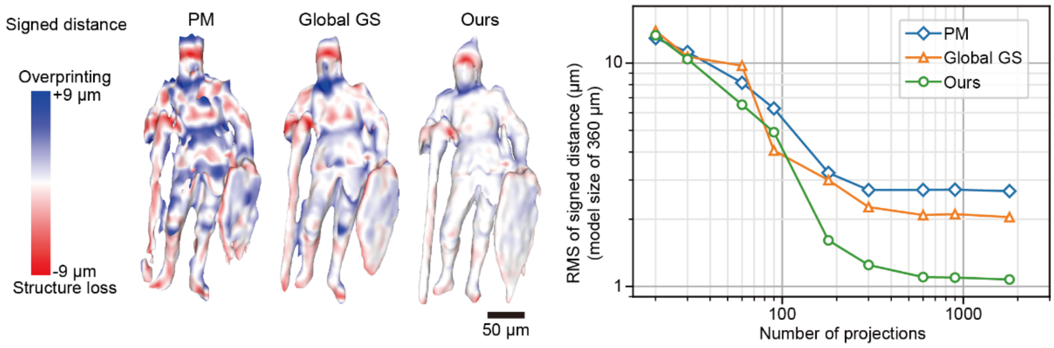

Figure R12: Signed distances of the simulated products of multiple pattern-optimization algorithms. (Fig. S6c) The signed distances of the simulated printing results, compared with the ground truth (1,800 binary projections used). Curves of the root mean square (RMS) of signed distances versus the number of total binary projection patterns used for different algorithms are shown on the right. The demonstrated model size is 360 μm and the pixel size for simulation is 1.8 μm.

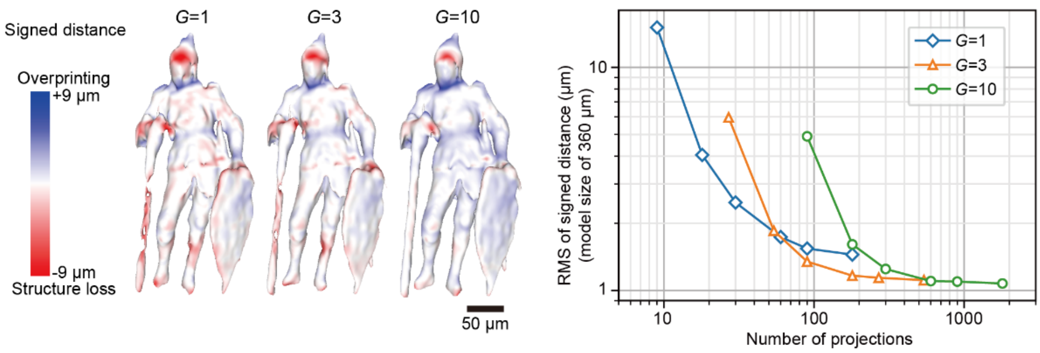

Figure R13: Signed distances of the simulated products of multiple binarization parameters. (Fig. S7b) The signed distances of the simulated products, compared with the ground truth, corresponding to 1, 3, and 10 binary projections as a group, corresponding to the binarization parameters G=1, 3, and 10. Curves of the RMS of signed distances versus the number of total binary projection patterns with different binarization parameters are shown on the right. The demonstrated model size is 360 μ m and the pixel size for simulation is 1.8 µm.

-- In Supplementary Figure 6a and 6b, the panels are labelled "intensity of the cross-sections" where I think dose distribution is meant. Again the difference between a 2D optical pattern and a 3D volumetric quantity is being confused here.

Response:

We thank the reviewer for pointing out these errors. The label has been revised to "dose distribution of the cross sections."

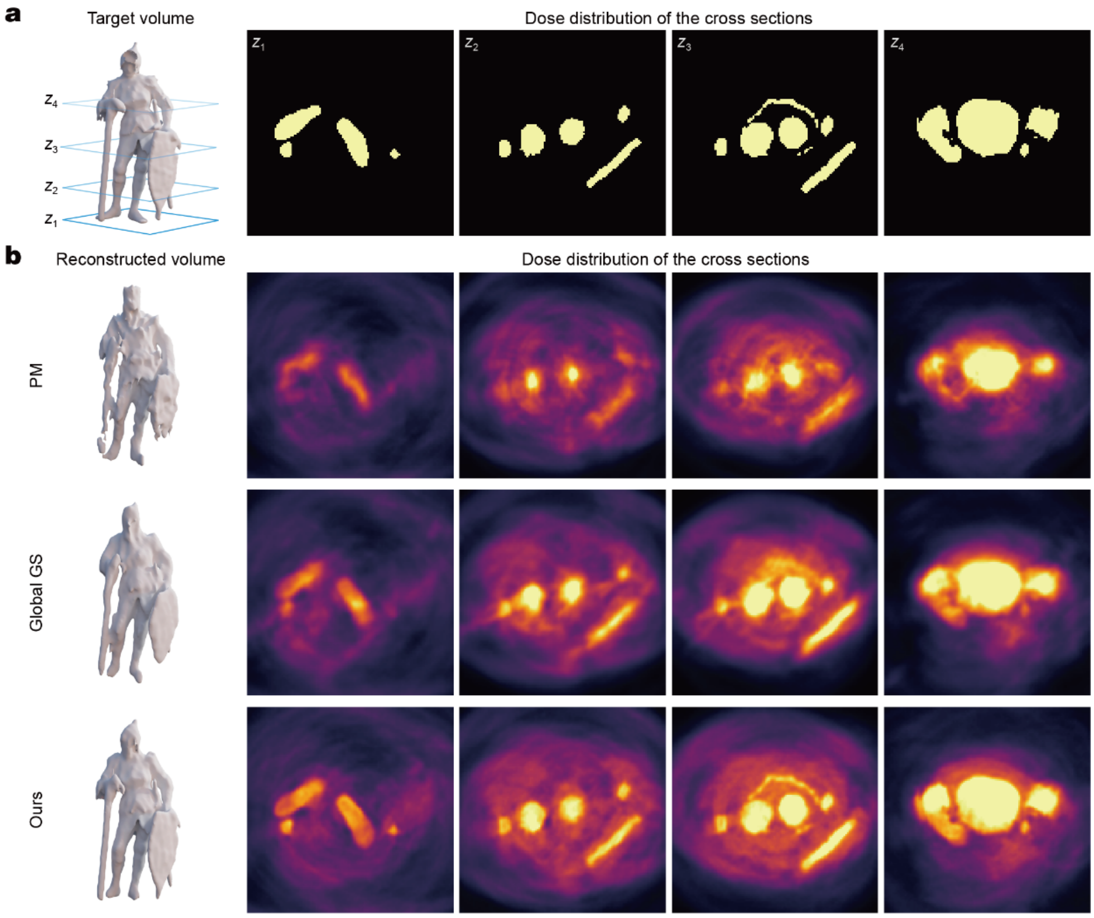

Figure R14: Comparative analysis of multiple pattern-optimization algorithms. (Fig. S6a-b) a, Illustration of the ground truth target volume and its cross-sections. **b,** Simulated printing results obtained by multiple optimization methods illustrated with their cross-sections. The methods include penalty minimization (PM) used in previous CAL methods with ray optics modeling, the global Gerchberg-Saxton (GS) algorithm, and our binary holographic optimization algorithm.

-- In Supplementary Fig 8, some of the text is too small to read, please increase the size.

Response:

We thank the reviewer for the thoughtful reminder. Inappropriate fonts have been revised in Supplementary Figure 8.

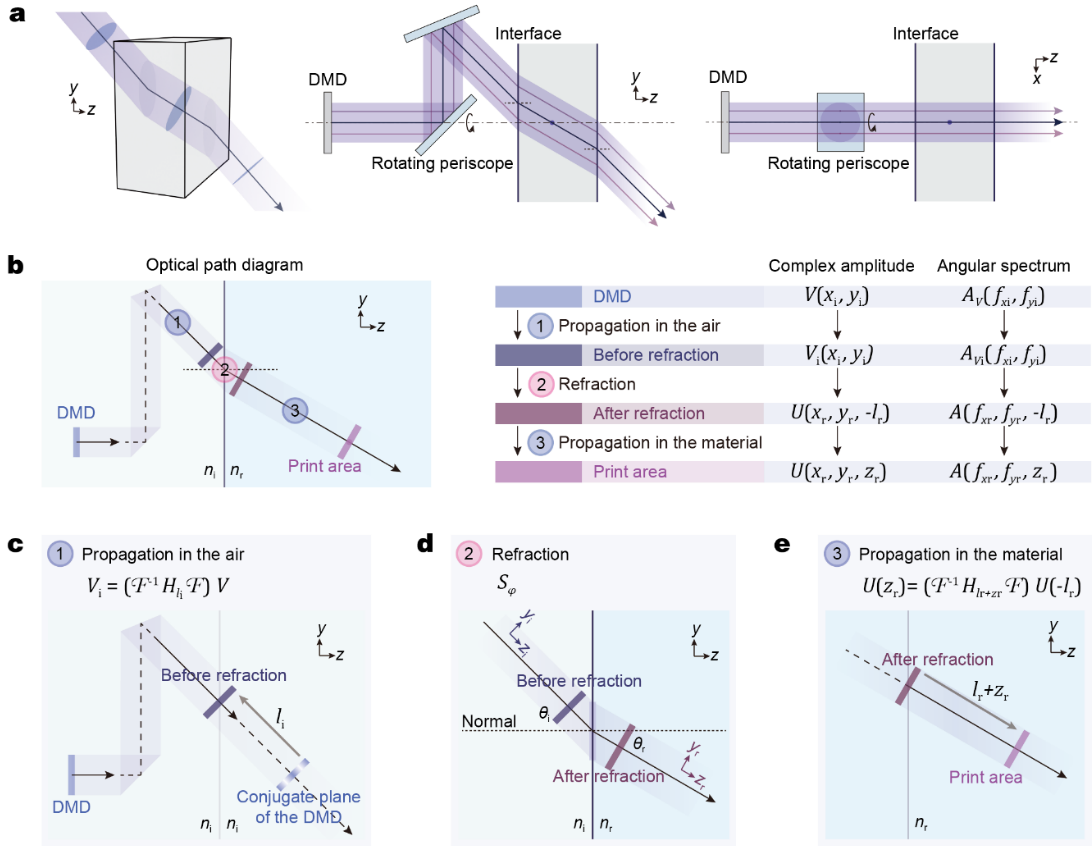

Figure R15: Wave-optics model of the beam propagation in DISH. (Fig. S8) a, Illustration of the beam path of DISH for a specific angle. As illustrated from different viewpoints, the refracted beams are stretched along one axis due to refraction and are less affected on another axis. **b**, The optical path diagram illustrates three stages of the beam propagation process during modeling, including propagation in air, refraction at the interface, and propagation in the material. **c**, Illustration of stage 1: propagation in air. Considering the 4f-system, air propagation is modeled as the Fresnel propagation from the DMD's conjugate plane back to the air-material interface. **d**, Illustration of stage 2: refraction at the interface. The beam's propagation direction alters based on the refraction theory, and the beam's complex amplitude is stretched. **e**, Illustration of stage 3: propagation in the material. The beam propagation is modeled as Fresnel propagation from the interface to the specific printing area within the material. θ_i represents the incident angle, θ_r represents the refracted angle, n_i represents the refractive index of the air, n_r represents the refractive index of the material, l_r represents the distance from the interface to the printing center, and z_r represents the distance from the printing center to the target location.

-- Lines 503-513 describing the 3D display capability, together with the Supplementary Figure 13 seem a little out of place. This is a nice additional capability but ultimately not related to the main point of the paper. I recommend removing it, unless they are critical to understanding other parts of the printing/calibration process.

Response:

We thank the reviewer for this thoughtful suggestion. The description and figure of the 3D display have been removed.

Referee #2

The scope of this paper is a volumetric projection technique termed digital incoherent synthesis of holographic light fields (DISH) and its use in additive manufacturing. This concept builds on volumetric projection techniques, most notably computed axial lithography (CAL) which is the current state-of-the-art in volumetric printing. On of the trade-offs in CAL is the fact that the volumetric projection reconstruction requires the illumination under various angles which is generally implemented by rotating the sample while leaving the projection source (usually a dynamic light patterning device such as digital micromirror device, DMD) stationary. This is the de facto gold standard given that the rotation of the light source is, instrumentally speaking, significantly more challenging. This sacrifices speed for commodity. As speed emerged as one of the most important criteria in volumetric additive manufacturing (VAM), the community investigated methods for speeding up the technique further. Various concepts have been explored and (at least theoretically) described. The technique presented in this work uses a rotating periscope. While this approach has been mentioned, the reviewer is not aware of an actual implementation and certainly not at the time scales demonstrated in this work.
To make one point very clear: This paper is an impressive improvement over the current state-of-the-art and merits publication in Nature. There are a couple of points which should be added and/or complemented in order to strengthen some aspects of the work.

Response:

We highly appreciate the reviewer's positive feedback and are pleased to know that the reviewer recognizes our advancement in increasing the speed of high-resolution volumetric printing. In the following sections, we address the specific concerns raised by the reviewer to further improve the manuscript and clarify key aspects of our work.

- We conducted new tests about the achievable printing resolution of DISH. New printing results indicate that the overall printing resolution is about 19 μm for diverse structures and the finest positive feature is measured as about 12 μm. Samples with sharp edges and intended angles were also printed.
- We characterized the beam profile from the DMD as required.
- We explained the stability, computational cost, and efficiency of the holographic algorithm in detail.
- We revised the texts regarding diverse material.

It would be good to include a measure of achievable precision. This is still a major point of concern in VAM and has been at the center of attention of the community. In general, we found that precision requires more gentle and extended illumination in order to achieve contrast. DISH is very fast and thus, it would be important to gauge, how precise the structures produced can be. This is particularly true as the examples given (including the videos) show components which are convectively moved during polymerization and thus, the precision does not only depend on the illumination but also the ambient transport conditions (convective ad- and off-transport of monomers, etc.). In order to assess this, it would be good to generate a test pattern with defined geometries. This pattern should be printed and measured to assess achievable precision and resolution. Mind you, it is not necessary to do this volumetrically, i.e., using tomography or the likes. A simple 2D test pattern (which can be checked using a microscope) would be entirely sufficient.

Response:

We sincerely appreciate the viewer's insightful comments and considerate suggestions. New models were designed to test the achievable precision. The relevant description has been revised in the abstract, introduction, results, and so have Figure 4 and Supplementary Figure 10.

In our previous results, we have shown the relief-sculpture texture with a width of 11 μm on a large sample. For better characterization of independent positive features, a fishbone model with designed rib widths of 2 pixels (10.8 μm) was printed, and the measured independent printed width is 11.9±2.1 μm (Fig. R16 and Fig. 4h-i). A more complex 3D model with the shape of a conch was also printed, with the lines in different directions and z-axis positions (Fig. R17 and Fig. 4l-o). The line widths in zoomed figures are measured as 19.3±3.4 μm. There are jagged edges on the line structures, which are mainly due to the pixel aliasing error caused by the 5.4-μm pixel size used in the modeling process. The difference between these results and the optical resolution/textured resolution may be caused by convection. Therefore, in our revised manuscript, we have updated our printing resolution of 19 μm for diverse structures, and mentioned that we can achieve the finest positive feature of about 12 μm. All the statements in the revised manuscript have been updated.

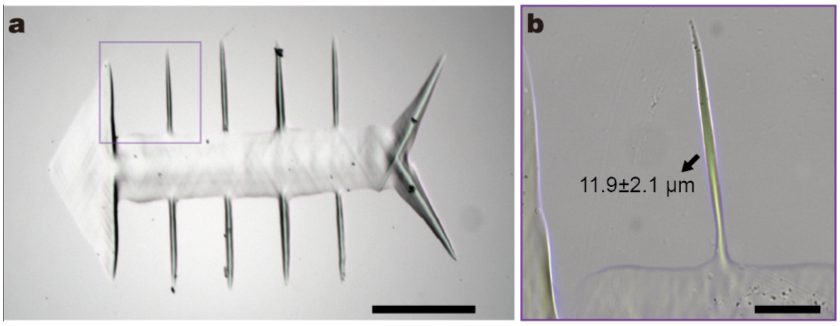

Figure R16: Fishbone model for the positive feature test (Fig. 4h-i) a, Printed fishbone model with designed rib widths of 10.8 μm. **b,** Close-up view of (a). The measured rib width is 11.9 ± 2.1 μm, representing the finest printable positive features of DISH. Scale bar: 500 μm (a) and 100 μm (b).

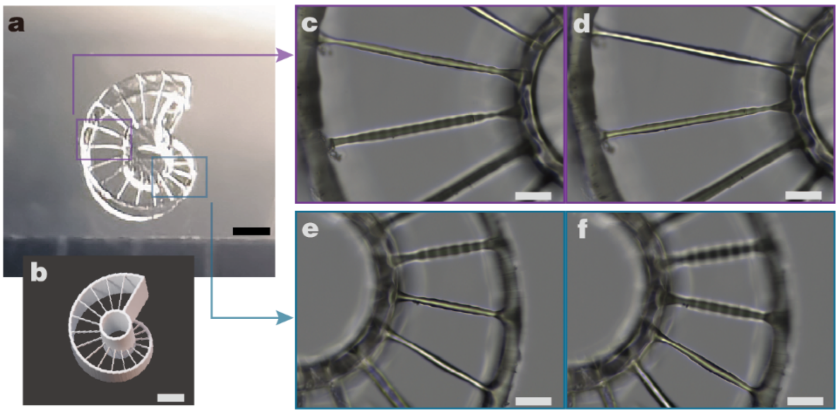

Figure R17: Conch model for comprehensive resolution test. (Fig. 4l-o) a-b, Conch model and its printout. Lines are arranged along different directions and z-axis positions. **c-f,** Close-up views of distinct lines. As the lines are distributed across z-axis positions, those outside the microscope's focal plane appear as defocused patterns. The measured width of these lines is 19.3 ± 3.4 μm. This model enables the characterization of the stable resolution achievable by DISH at various positions when printing more complex structures. Scale bar: 500 μm (a-b) and 100 μm (c-f).

The structures shown do not feature sharp edges. All hard corners seem rounded off. All images in Fig. 4 seem organic, even the airplane has rounded corners where the digital model would have a hard edge. It would be good to assess, how well DISH can produce hard edges and intended angles (30deg, 45deg, etc.). Again, a sample structure would be sufficient here.

Response:

Thanks for the reviewer's constructive comments. Several structures with sharp edges and intended angles have been printed, as illustrated in Fig. R18.

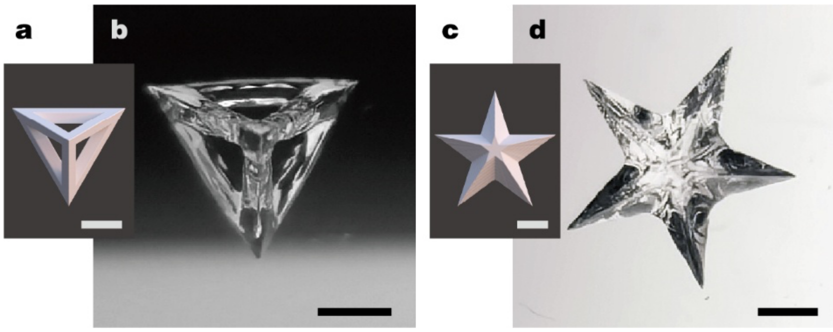

Figure R18: Structures with sharp edges printed by DISH (Fig. 4j-k). **a-b**, Triangular pyramid frame model and its corresponding printed result. The printed object exhibits sharp edges. **c-d**, Five-pointed star model and its corresponding printed result. Each angle of the model is designed to be 36°, while the measured angle of the printed result is 36.0 ± 1.6°. Scale bar: 1 mm.

Previously, we ignored that sharp edges are important features revealing resolution, so many models have cylindrical edges or rounded corners during design. Now these printouts have been added as Fig.4j-k.

Please indicate the irradiance (i.e., intensity per area) of the light source as well as the beam profile emitted from the DMD. For this, an intensity scan (in the easiest sense with a CMOS or CCD chip) should be recorded on the DMDs projection beam when the DMD is set to all white. It would be important to know how uniform the projection needs to be.

Response:

We sincerely appreciate the reviewer's comment. We mounted an attenuation filter on the camera and focused it on the DMD to obtain the relative intensity distribution corresponding to each pixel of the DMD. Subsequently, by projecting a square pattern of 1×1 mm^2 and measuring its total power with a power meter, the absolute intensity is derived as follows:

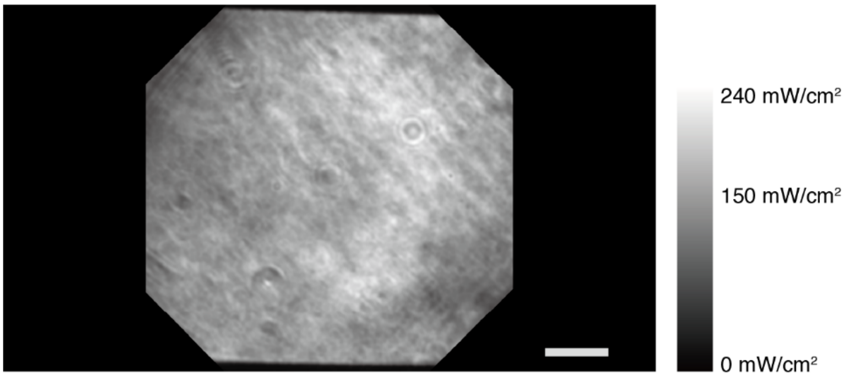

Figure R19: The measured intensity distribution with all DMD pixels being set to white. The intensity distribution is not uniformly distributed in practice. These non-uniformities have been calibrated by the optimization algorithm to achieve various desired intensity distributions. Scale bar: 1 mm.

Fig. R19 corresponds to $|u|^2$ in the paper. The intensity non-uniformity has been calibrated in our algorithm, as the projected complex amplitude is formulated as $\delta_\varphi u$ for the DMD pattern δ_φ.

Please elaborate on the need for the improved algorithm for the generation of the phase projection patterns. Obviously, the strength of the GS algorithm is neither its speed nor the chance of converging to a global maximum. It is used for its numerical stability (i.e., it is near-impossible to nor converge GS) as well as the fact that convergence can be proven, i.e., the algorithm will (almost) always find an optimum - even if its only a local one. Lastly, FFT and iFFT are fast and very convenient to scale on commodity hardware which makes GS optimization affordable. How does this algorithm compare in terms of stability and cost (i.e., what is the big O scaling of the algorithm?)? How long does pattern prepreparation take and which hardware is required? This is still a bottleneck in conventional CAL as the time needed to derive the sinograms is significantly longer than, e.g. a slicer would take.

Response:

We thank the reviewer for this valuable and multifaceted question. Compared to traditional non-holographic algorithms, our approach does require additional computational time for improved projection precision. This extra computational cost associated with improved resolution is indeed not ideal for practical implementation. However, we anticipate that the algorithm's efficiency can be substantially enhanced through future development, for instance, the integration of deep neural networks.

Regarding the algorithm's stability, Fig. R20 illustrates the relationship between the number of iterations and the Jaccard index for our algorithm, in comparison to the Global Gerchberg-Saxton algorithm, using the Theodoric model. Our algorithm exhibits a rapid increase in the Jaccard index within the first 10 iterations, followed by a convergent increase.

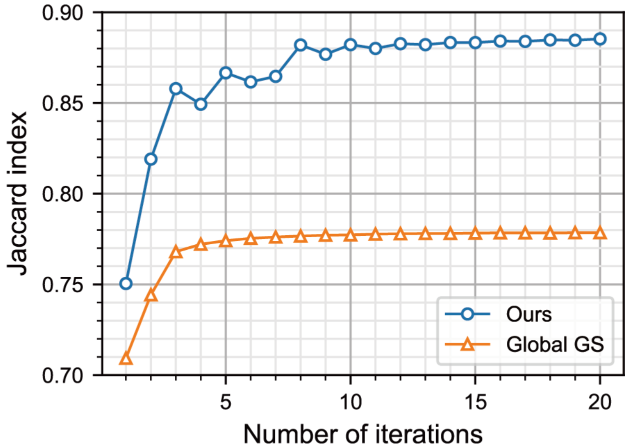

Figure R20: Curves of the Jaccard index between the simulated products and the target, versus the number of iterations of Global GS and our algorithm. Using Theodoric as the target model, both Global GS and our algorithm exhibit a rapid increase in the Jaccard index within the first 5 to 10 iterations, followed by a convergent increase. Our algorithm exhibits a slower convergence rate but achieves a significantly higher Jaccard index than the Global GS method.

Concerning the algorithm's computational cost, the temporal complexity of our algorithm is $O(V \cdot T \cdot G \cdot MN^2 \log N)$, where V represents the number of coarse viewing angles, T represents the number of iterations, G presents the binarization parameter, M represents the number of volume layers after axial down-sampling, and $O(N^2 \log N)$ corresponds to the time complexity of the 2D Fast Fourier Transform. Specifically, the most time-consuming step is the forward propagation, that is, calculating the 3D dose of G binary images. For computing the light intensity distribution of a single layer, according to the propagation formula: $\mathcal{H}_\varphi(z_\mathrm{r}) = \mathcal{F}^{-1} H(z_\mathrm{r} + l_\mathrm{r}, \lambda_\mathrm{r}) \cdot S_\varphi \cdot H(l_\mathrm{i}, \lambda_\mathrm{i}) \mathcal{F}$, the most computationally intensive components are the 2D FFT and 2D iFFT. Therefore, propagating all G images requires $O(GMN^2 \log N)$. Another time-consuming step is finding the descent direction, where the most time-consuming part is the backpropagation $\mathcal{H}_\varphi^{-1}$. This step propagates each layer of the volume separately before summation, with a time complexity identical to the forward propagation of a single pattern, that is, $O(GMN^2 \log N)$. The time complexity of all other steps does not exceed the above. Thus, the total time complexity for one loop is $O(GMN^2\log N)$. In experiments, for a model with dimensions of 1350×1350×1852, it takes about 24 hours to complete under the following parameters: N=1350, M=20 (corresponding to a resampling interval of 500 μm), G=10, V=180 coarse viewing angles, and T=20 iterations.

While current 3D holographic algorithms are inherently time-consuming, our approach still exhibits competitive efficiency relative to existing methods. In the paper *Wave optical model for tomographic volumetric additive manufacturing*, processing 550×550×550 voxels with 600 angles took 4 hours on an NVIDIA A100 with 80GB GPU RAM. In contrast, our algorithm processes a 1350×1350×1852-voxel volume across 1800 angles in 24 hours without GPU acceleration. Notably, our voxel count is 20-fold higher than that of the aforementioned method, yet our runtime is only 6-fold longer, demonstrating that our algorithm would require less time for an equivalent voxel volume. Nevertheless, we acknowledge that its computational cost remains prohibitive for practical applications.

We hypothesize that holographic algorithm efficiency can be substantially enhanced via the integration of deep neural network in the future. For instance, the end-to-end neural network approach presented in *End-to-end learning of 3D phase-only holograms for holographic display* accelerates 3D hologram generation to about 5 frames per second, which can be applied in our framework in the future to accelerate the computing process. We have added this limitation in the discussion and pointed out the potential solutions with deep learning.

The revised paragraphs include: "As for the computational cost of the algorithm before the printing process, DISH is comparable to other computed holographic methods[25]. Still, after acquiring high-resolution datasets that account for refractive aberrations, introducing end-to-end neural networks for 3D hologram generation[40,41] and GPU acceleration may greatly reduce the computational cost." (line 314)

I would also tune down the claim on diverse materials. All of the materials shown are all (meth)acrylates. In order to claim diverse materials, it would be necessary to add also ionic materials (such as, e.g., epoxy-based), thiol-ene or other type of additive-type polymers. This is not a major point of concern, VAM currently mostly investigates acrylates - but this is not a particular achievement of this paper and thus, this claim should either be complemented or tuned down.
In summary: This is an impressive piece of work which merits publication after the given points have been amended.

Response:

We sincerely appreciate the viewer's thoughtful suggestion. The phrase "diverse materials" was intended to show that we used materials of a larger viscosity range compared to other volumetric printing works, including several commonly used molecules in 3D printing. Now we have updated the subtitles and replaced "diverse materials" with "different materials". Just as you mentioned, the application of diverse materials is not a major point of this work, so we did not test other additive-type polymers. But for future work, we think thiol-ene-based materials are good choices as they have been successfully used in volumetric printing and could meet many functional requirements of bioprinting. However, ionic polymerization alone may not be an advantageous scenario for DISH, due to the relatively slow reaction rate. Currently, the ionic ink for layer-wise printing takes at least a few seconds per layer to cure, so it can barely be printed volumetrically within ten seconds.

Referee #3

The manuscript by Wang et al., titled "Sub-second Volumetric Additive Manufacturing by Digital Incoherent Synthesis of Holographic Light Fields" is timely and aligns with the significant progress made since the development of computed axial tomography (CAT), xolography, and acoustic field-based techniques for volumetric 3D printing. The method shares striking similarities with CAT, where pre-calculated 2D light patterns are projected into a volume to generate a targeted 3D light dose that induces photopolymerization within the desired region. However, instead of rotating the vat to allow radiation from different angles, the light beam is directed by a rotating periscope system, which enables it to enter from various orientations, while the vat remains stationary. This enables faster application of the angular projections and thus printing with low-viscosity resins, where the objects would otherwise be deformed by gravitational sinking. Although the movement of the optical components poses a challenge for the precise superimposition of the individual projections in the cuvette, the authors were able to solve these problems through fluorescence imaging and the use of adaptive optics. They pursue the approach of radiating several projections for each angular range in order to generate structures with higher resolution outside the depth of field of the objective. Wave-optical modelling and iterative algorithms are developed to optimize angular projections. Supplementary video 1 and 2 show the fast object creation and 3D printing in the flow.

The method is based on the principles of CAT, so its novelty is not particularly groundbreaking. Additionally, the paper currently lacks sufficient data and results, so I do not recommend publishing it directly in Nature. However, if the points discussed below are effectively addressed in a major revision, I would support its publication in one of the sub-journals of the Nature portfolio, as the results could be impactful in the field of volumetric 3D printing and of interest to a broader audience.

Response:

We greatly appreciate the reviewer's constructive comments. The resolution and fidelity are critical factors for volumetric printing, and an in-depth description of the projection and algorithm is important for the illustration. In the following sections, we address the specific points raised by the reviewer to further improve the manuscript and clarify important aspects of our work.

- We explained why 45° was chosen as the incident angle and the impact of missing cone in printing resolution and fidelity, and added data about experimental optical resolution. We also revised inaccurate words about 360 degrees and explained the obstacles for a vertical projection version of DISH.
- We specified the building volume and its influence factors, and updated the relevant texts.
- We conducted new tests and better characterized the experimental printing resolution. New printing results indicate that the overall resolution is about 19 μm and the finest positive feature in specific models is measured as 12 μm. Relevant new results and discussion were updated.
- We added the digital model in Fig.1b for direct comparison of shape fidelity and provided a video to show the post-printing step and the mechanical stability of our products.
- We further clarified our holographic optimization algorithm in detail with the comparisons to the control group methods, including PM and Global GS.
- We updated the introduction texts referring to Xolography, labeled the simulation results in Fig. 1, and cited the new review on volumetric printing.

1) Limited Angle Projections / Missing Cone Problem:

In CAL, the resin vessel is rotated 360 degrees, allowing projections to enter the vat from all directions. This is crucial for ensuring the accuracy and fidelity of the resulting shape. As shown in Suppl. Figure 3, the light beam always enters the cuvette through one of its side windows at a 45-degree angle relative to the surface normal. As the beam rotates, it irradiates a cone that covers a solid angle of about 0.6π in air. In the cuvette, the cone is even smaller, as the light beam is refracted toward the normal line due to the increase in refractive index at the air-cuvette-resin interface.

The authors frequently refer to a "360-degree projection," as stated on page 4, line 71: "…to deliver a 360-degree high-resolution projection of precisely controlled light fields at …,” and on line 78: “…then developed to optimize 360-degree holographic patterns …,” and line 95: “in DISH to facilitate 360-degree projections,” among others. While the periscope makes full rotations, referring to the angular projections as 360 degrees is misleading and should be corrected.

Response:

We sincerely appreciate the reviewer's insightful comments. Our periscope rotates 360°, but the term “360-degree” applies exclusively to rotation about the z-axis, not to other axes. In response to this valuable suggestion, we have revised the relevant sentences to prevent confusion: line 74 “we design a ~~360-degree~~ rotating periscope with long-working-distance 0.055-NA objective to deliver high-resolution projection”; line 81 “An iterative algorithm … is then developed to optimize the holographic patterns corresponding to different angles …”; line 98 “we develop a rotating periscope in DISH to facilitate high-speed angular projections …”

It would be valuable to provide a theoretical analysis of how projections from a limited set of angles affect resolution and shape fidelity. Additionally, it would be helpful to explain why a 45-degree angle was chosen instead of a larger angle.

Response:

We thank the reviewer for the constructive suggestions. The following explanations address three aspects: the impact of oblique projection on resolution, an analysis of its effect on shape fidelity, and the considerations determining the incident angle. We have added corresponding illustrations in the revised manuscript.

(1) Impact of oblique projection on resolution

The theoretical lateral resolution is consistent with the projection resolution, while the theoretical axial resolution must account for the pattern stretching: after refraction, the maximum axial distance measurable for a beam of width d is $d/(\cos\theta_{\mathrm{i}} \tan\theta_{\mathrm{r}})$. This value does not represent the axial resolution itself but serves as a reference for it. In general, the axial resolution is poorer than the lateral resolution and is influenced by the material’s refractive index and the incident angle.

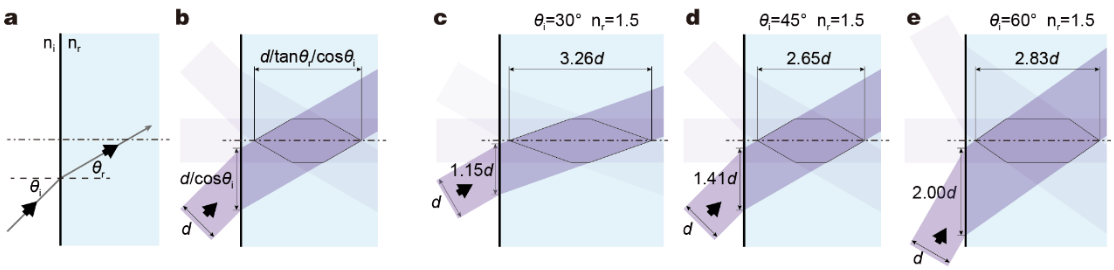

Figure R21: Impact of oblique projection on axial resolution. a, Definitions of the refractive index of air (n_i), the refractive index of the material (n_r), incident angle (θ_i), and refractive angle (θ_r). **b**, When a light beam with diameter d is incident at θ_i, the distance measured at the interface is $d/\cos(\theta_i)$. After the beam refracts into the container, its axial distance is $d/\cos(\theta_i)/\tan(\theta_r)$. This axial distance cannot be equated to the actual axial resolution, but it can serve as a theoretical reference for axial resolution. Generally, the shorter this axial distance, the better the axial resolution. **c-e**, Axial stretching of the light beam under different incident angles. Either excessively small or excessively large incident angles are unsuitable. The axial distance reaches its minimum value at a specific incident angle determined by the material's refractive index.

The actual projectable feature size should be determined by experimental results. Dense dot arrays are projected in a coumarin-DMSO solution with a refractive index of 1.48 ($1/(\cos\theta_i \tan\theta_r)$=2.60, and 5.4 μm × 2.60=14.04 μm in this case), and the captured fluorescence images from the front and side are shown in Fig. R22 (Fig. S9e). The lateral resolution did not reach the DMD pixel size of 5.4 μm, primarily due to the limit of the calibration methods. Our pixel-level calibration method cannot ensure sufficient contrast for 1-pixel patterns, resulting in a minimum projectable lateral size of two DMD pixels. Axially, the target pattern is distinguishable for 22.1 μm, which is poorer than the lateral resolution.

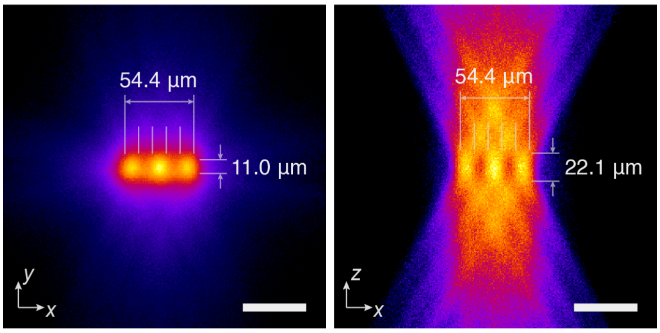

Figure R22: Experimental measurement of the voxel (Fig. S9e). Our voxel is defined as the bounding cuboid of the smallest clearly distinguishable projected point. A dense dot array pattern was projected into a coumarin-30 fluorescent solution, and their 3D dimensions were measured to be $(11.0\ \mu m)^2 \times 22.1\ \mu m$. Scale bar: 50 μm.

(2) Analysis of the impact of oblique projection on shape fidelity

Shape fidelity can be more effectively analyzed in the 3D Fourier domain for our system. Under ideal conditions (no beam attenuation or diffraction), a single beam can only populate information within the plane perpendicular to its propagation direction in this domain. Thus, the current oblique projection can only provide information where the angle relative to the z-axis is greater than $\pi/2-\theta_\mathrm{r}$, creating a missing cone around the z-axis. This implies that, in the absence of attenuation, any shape containing information along the z-axis in the 3D Fourier domain, such as a cuboid, cannot be projected.

In practice, however, beams undergo obvious attenuation within materials: their intensity diminishes as the distance from the material's front surface increases. This attenuation is equivalent to multiplying the 3D dose by a z-dependent exponential decay function, defined as $f(z)=e^{-\mu' z}\cdot\mathrm{rect}\{z/z_0\}$. This is equivalent to convolving with a kernel $\mathcal{F}\{f(z)\}=\mathrm{Const}\cdot\frac{1}{\mu'+j\omega_z}*\mathrm{sinc}\left(\frac{z_0\omega_z}{2\pi}\right)$ in the 3D Fourier domain. This convolution populates significant low-frequency components within the missing cone, thereby enabling the printing of structures like cuboids. Nevertheless, since the frequency components within the missing cone depend mostly on intensity attenuation for their population, structures containing high-frequency information along the z-axis in the 3D Fourier domain, for instance, repeated stacks of thin xy-planes, remain unprojectable.

(3) The incident angle is selected by considering two factors: minimizing the axially projectable feature size from one side and reducing energy loss from interface reflection.

Optimal axial feature size can be achieved when the incident angle is close to the value determined by the material's refractive index. In ray optics, the axial distance of a refracted beam of width d becomes $d/(\cos\theta_\mathrm{i}\tan\theta_\mathrm{r})$. Defining the coefficient $S=1/(\cos\theta_\mathrm{i}\tan\theta_\mathrm{r})$, differentiation shows that S is minimized when $\sin\theta_\mathrm{i}=\sqrt{\frac{1-\sqrt{1-(n_\mathrm{i}/n_\mathrm{r})^2}}{(n_\mathrm{i}/n_\mathrm{r})^2}}$, where n_i (refractive index of air) is 1, and n_r is the material's refractive index. A larger n_r shifts the optimal incident angle closer to 45°. For materials with a refractive index of ~1.5 (mostly used in this study), S reaches a minimum of 2.62 at 49°; $S \leqslant 2.65$ for incident angles between 45° and 54°, and S fluctuates less in this range.

Energy loss from interface reflection generally increases with larger incident angles. Since the projecting angle varies relative to the polarization direction in our system, the efficiency of refracted light is calculated as the average of p-polarized and s-polarized light: $T=1-\left(\left(\frac{\sin(\theta_\mathrm{r}-\theta_\mathrm{i})}{\sin(\theta_\mathrm{r}+\theta_\mathrm{i})}\right)^2+\left(\frac{\tan(\theta_\mathrm{r}-\theta_\mathrm{i})}{\tan(\theta_\mathrm{r}+\theta_\mathrm{i})}\right)^2\right)/2$. When both the container and material have a refractive index of 1.5, the efficiency is 95.0% at 45°, 94.4% at 49°, and 93.3% at 54°.

Therefore, the incident angle of 45° was selected to reach the highest axial resolution printable from one side and maximize the refractive efficiency.

The authors propose an alternative design, shown in Suppl. Fig. 12, to solve the problem of the missing cone, but no further results have been published. As this approach is introduced into the conclusion section, it should be described why this has not been implemented so far and what are the obstacles to realize it.

Response:

We thank the reviewer for this insightful question. The primary current challenge arises from replacing the container's planar interface with a curved one; this causes beams entering the container to converge, rendering the angular spectrum propagation model much more complicated for high-precision calculation, degrading the experimental printing performance. Although the propagation direction of beams can be readily calculated under ray optics, the substantial variation in this direction violates the paraxial approximation essential for angular spectrum modeling. Specifically, an extremely high spatial sampling frequency would be required to characterize the phase modulation induced by the curved surface during calculation. Consequently, the algorithm used in this work is no longer viable, and both aberrations and depth of field must be re-evaluated to ensure the resolution of printed structures. All these problems raise substantially higher requirements for the computational costs, which preclude its practical application at the current stage. Integration of a deep neural network may address this problem by increasing the calculation speed and precision. We have revised the relevant paragraph in the discussion section.

Another approach to avoid the curved interface is to use an additional container filled with refractive index-matching fluid, which rotates synchronously with the optical path. This approach is identical to that of traditional volumetric printing but necessitates a completely redesigned mechanical system.

The revised paragraphs include: "Changing the mechanical design of the periscope can address this problem (Supplementary Fig. 12). However, the significant variation in propagation direction for curved container surfaces violates the paraxial approximation required for angular spectrum modelling, where an extremely high spatial sampling frequency is needed to model the phase modulation process induced by the curve surface during calculation. Consequently, higher computational costs would be required, and both aberrations and depth of field should be re-evaluated to ensure the resolution of printed structures in this mechanical design." (line 340)

2) Build-Volume Size:

The superposition of the individual beams, each with a 6mm diameter, within the cuvette defines the build volume within the resin space. Based on the schematic in

Suppl. Figure 2, the build volume in the y,z plane resembles a rhombus, which could significantly reduce the available print volume depending on the shape of the object being printed. The authors demonstrate the fabrication of objects, as shown in Figure 1 and Suppl. Figure 10, with dimensions of approximately 7-8mm in the z-axis and a maximum of 3-4mm in the x and y axes. However, they mention the printing of centimeter-scale objects, for example, in the abstract (page 2, line 31), the main text (page 3, line 50), page 4 (line 66), page 7 (line 118), and several other places throughout the manuscript. Based on the demonstrated fabrication sizes, the proposed setup appears to allow printing of millimeter-scale objects only and the manuscript should be updated accordingly. The shape and size of the available build volume are not discussed in detail. On page 4, the manuscript briefly mentions "…the entire 1 cm^3 volume …," while in the conclusion (line 273), it states: "By DISH, a sample with a volume of approximately 200 mm^3 can be produced in …." There is a discrepancy of a factor of 5 between these two values, which should be clarified. It would be helpful to provide the dimensions of the build volume (in the x, y, z axes) as a function of the central design parameters of the periscope and illumination geometry.
What are the main factors that currently limit to increase the build volume?

Response:

We sincerely appreciate the reviewer's insightful comments on build volume. Our build volume is 200 mm^3 and the maximum dimension is 10 mm in z-axis and 5.8 mm in x and y axes. The detailed calculation and discussion of the build volume are as follows:

The build volume of 200 mm^3 is calculated based on the volume that is irradiated by beams from all angles. As shown in Fig. R23, when the DMD always projects a circular pattern, the printing area is a centrally symmetric spindle shape, which can be approximated by a cylinder and two cones. The volume of the cylinder is $\pi\left(\frac{d}{2}\right)^2 \cdot \frac{d}{\tan\theta_r}\left(\frac{1}{\cos\theta_i}-1\right)$, and the volume of two cones is $2\cdot\frac{1}{3}\pi\left(\frac{d}{2}\right)^2\cdot\left(\frac{d}{2\tan\theta_r}\right)$. The total volume is thus $\frac{1}{4}\pi d^3\frac{1}{\tan\theta_r}\left(\frac{1}{\cos\theta_i}-\frac{2}{3}\right)$, where d is the beam diameter, θ_i is the incident angle, and θ_r is the refracted angle. The short side length of the DMD is 1080 ×10.8 μm = 11.664 mm, and after 2x beam reduction, the beam diameter is d=5.832 mm. When the refractive index of the material is 1.48, the refraction angle θ_r≈28.54°, and the volume is 214.1 mm^3. Since the shape is not a strict combination of a cylinder and cones, and the spindle vertices are often unused, we estimate the printing region to be 200 mm^3. Additionally, because the shape of DMD is rectangular and the periscope design allows a maximum beam diameter of 6 mm to pass through, the final printing area will include some additional irregularly shaped areas.

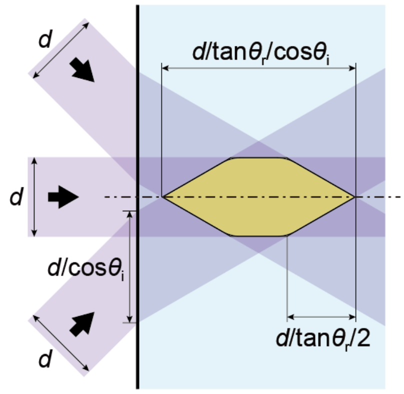

Figure R23: Shape of the printing area (Fig S3c). The printing area of the system is defined as the region illuminated by light beams from all angles. When the light beam has a circular cross-section with diameter *d*, the printing area approximates a spindle-like structure. When its volume is approximated using a cylinder and two cones, the volume can be expressed as $\frac{1}{4}\pi d^3 \frac{1}{\tan\theta_r}\left(\frac{1}{\cos\theta_i}-\frac{2}{3}\right)$, where θ_i denotes the incident angle and θ_r denotes the refracted angle. When d=5.832 mm (the short-side width of the DMD is reduced by a 2× beam reducer)，the material refractive index is 1.48, and the incident angle is 45°, the approximated volume is calculated to be 214.1 mm^3.

The main factor influencing the build volume with the same printing resolution is the pixel number of the DMD projector. Now we use only a 1080P DMD projector with a small number of pixels. A 4K-resolution DMD device or using multiple projectors simultaneously can greatly increase the beam size and print volume without sacrificing resolution and printing speed.

The updated texts include:

1. All “centimeter-scale” has been revised to “millimeter-scale”, or deleted.

2. Line 298 Added determiner “throughout the container” for 1 cm. Here 1 cm refers to the z-axis scale and aims at comparing to the focal depth in geometry optics. Therefore, it was not deleted, but the determiner was added to avoid the misleading of building volume. So do line 87 the “1 cm depth”

3) Resolution:

The authors report the printing resolution in the abstract: “… in DISH maintains an 11-µm printing resolution across the 1 cm range.” However, on page 11, line 216, they state: “Finally, we quantitatively characterized the experimental printing resolution of

DISH at different axial positions by printing high-resolution stripes on the 3D surface. A model with an axial length of 1 cm was designed with featured lines of different widths on the surface, with the smallest line width of 10.8 μm corresponding to 2 DMD pixels (each pixel corresponds to about 5.4 μm at the objective plane)."

From the description, it remains unclear what type of "3D surface" was printed. The image in Fig. 3g suggests a thin rhombic model to fit the build volume. It appears that this model was deliberately chosen to demonstrate the smallest feature size based on the lateral spacing of DMD pixels, which are directly imaged onto a thin surface (a 2.5D object) without the presence of potentially degrading structures around it. This is not a reference object with extended geometry, and I would suggest fabricating a more representative model, such as a "benchy" model or common 3D resolution targets, including both positive (pins, rods) and negative (holes) features, to provide more convincing data on the achievable x, y, and z resolution.

Ideally, the characterization should be performed using SEM images, micro-computed tomography (CT), or profilometry data sets. Similar to CAL, the resolution seems to degrade as the object size and complexity increase. For example, looking at the other objects printed, as shown in Fig. 1b, they appear quite blurry, and the resolution seems to be significantly lower than 11 μm, likely in the 50-100 μm range.

In this context, the benchmarking of DISH in relation to other methods in Suppl. Figure 1 remains questionable.

Response:

We thank the reviewer for the constructive comments. Printing resolution is a critical consideration in tomography-based 3D printing, and we have therefore supplemented new experimental results and revised text to replace previously ambiguous expressions.

For positive features, we designed a fishbone model with rib widths of 2 pixels (10.8 μm). The printed product is shown below in Fig. R24 (Fig. 4h-i), with the measured rib width being 11.9±2.1 μm. For a more complex demonstration of printing capability, we fabricated a 3D conch model featuring lines with varying orientations and z-axis positions as shown in Fig. R25 (Fig.4l-o). The close-up measurements revealed line widths of 19.3±3.4 μm. Jagged edges were observed on these line structures, primarily attributed to pixel aliasing errors arising from the 5.4-μm pixel size employed in the modeling process. Additionally, we printed an unsupported 3D wireframe structure to further validate the system's printing performance, with its linewidth measured as 18.9±1.5 μm (Fig. R26). In summary, our system can print features with a resolution of 19 μm, with 12-μm positive features achievable in specific models. Accordingly, we have updated the experimental printing resolution value to 19 μm throughout the revised manuscript.

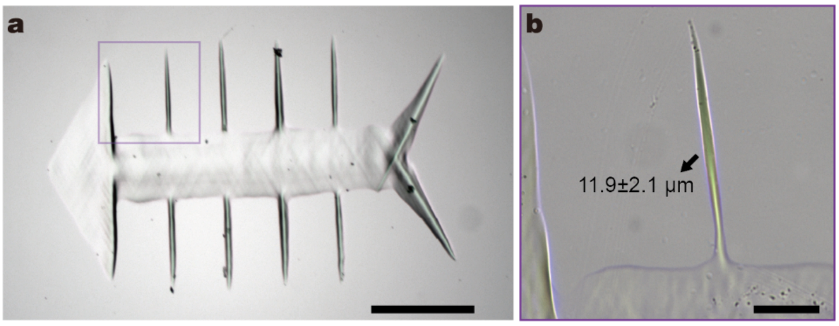

Figure R24: Fishbone model for the positive feature test (Fig. 4h-i) a, Printed fishbone model with designed rib widths of 10.8 μm. **b,** Close-up view of (a). The measured rib width is 11.9 ± 2.1 μm, representing the finest printable positive features of DISH. Scale bar: 500 μm (a) and 100 μm (b).

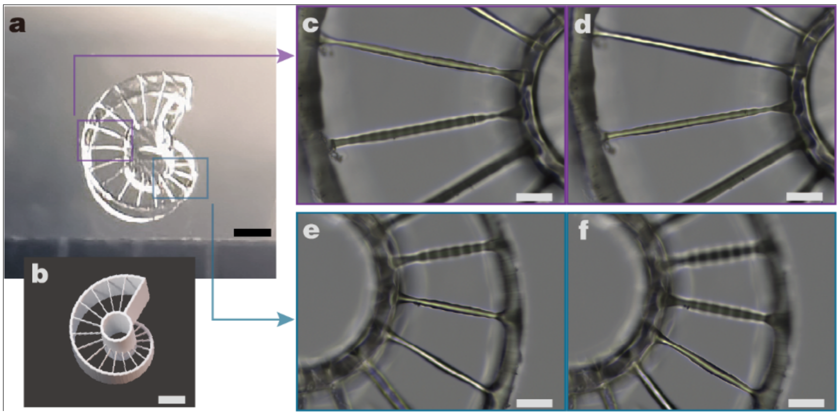

Figure R25: Conch model for comprehensive resolution test. (Fig. 4l-o) a-b, Conch model and its printout. Lines are arranged along different directions and z-axis positions. **c-f,** Close-up views of distinct lines. As the lines are distributed across z-axis positions, those outside the microscope's focal plane appear as defocused patterns. The measured width of these lines is 19.3 ± 3.4 μm. This model enables the characterization of the stable resolution achievable by DISH at various positions when printing more complex structures. Scale bar: 500 μm (a-b) and 100 μm (c-f).

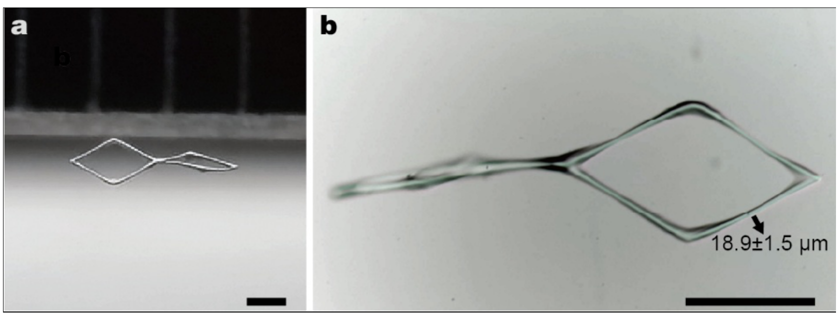

Figure R26: Unsupported wireframe structure. a, Sample imaged via a macro lens. **b**, Sample under a microscope. This unsupported wireframe requires higher dose contrast to print than samples with large solid bases. Scale bar: 500 µm.

For negative features, we printed an inner conical model, as shown in Fig. R27 (Fig. S10f-g). Injecting blue pigment allowed us to locate and measure the cone's vertex; the diameters of the inscribed circles at the vertices are 55.8 µm and 49.7 µm, respectively.

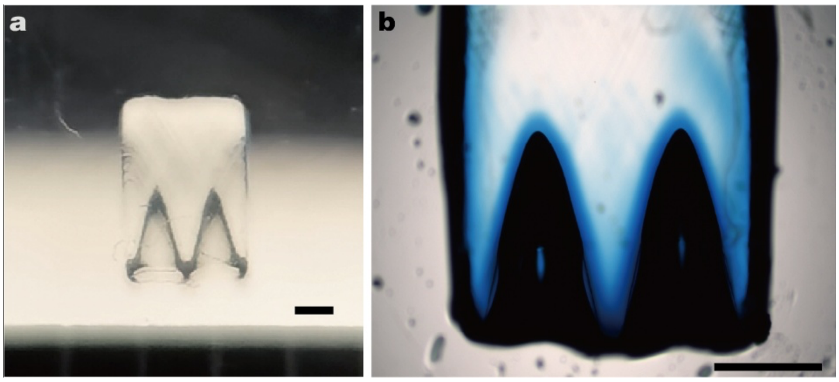

Figure R27: Inner conical model for negative feature test (Fig. S10f-g). After printing, the sample was injected with ink and imaged to verify the dimensions of the actually printed negative features. The diameters of the inscribed circles at the cone vertices are measured as 55.8 µm and 49.7 µm, respectively. Scale bar: 500 µm.

We also printed a "Benchy" model as shown in Fig. R28. This model was not used for resolution testing, as proportional downscaling resulted in thinner walls that could not support the relatively thicker structures, leading to deformation during post-processing.

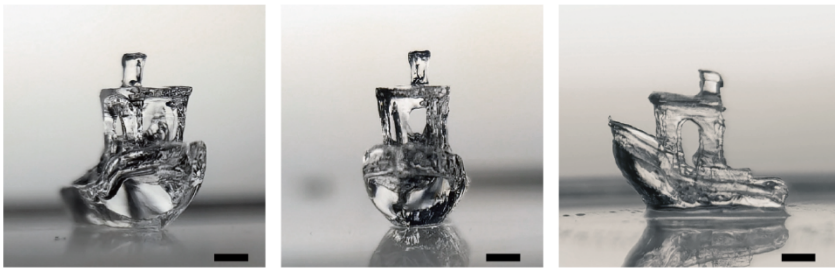

Figure R28: Benchy model printed by DISH (Fig. 5g, S11e). The Benchy test model was printed to verify the system's performance in fabricating complex models, and most structures of the Benchy model were successfully fabricated. This model was not used as a resolution test model because proportional downscaling resulted in thinner walls that failed to support the relatively thicker adjacent structures, leading to deformation during post-processing. Scale bar: 1 mm.

Relief models are sensitive to subtle dose contrasts, whereas unsupported small structures demand significantly higher dose contrasts. Since dose contrast in volumetric printing is constrained by projection conditions, optical resolution does not always align with the resolution of printed parts. In this case, the nonlinear curing characteristics of the material play a crucial role. As described in the paper *Deconvolution volumetric additive manufacturing*, the dose required to cure a given voxel is not constant and depends on the structure's size and geometry. Owing to diffusion effects, fine, sparse structures typically require a higher curing dose than bulk or dense structures, and they are also more sensitive to dose uniformity and contrast. This is why we designed the unsupported rhombic wireframe model as an extreme test case: it demands the highest dose contrast. In contrast, fine structures in relief models or details attached to a main structure require lower dose contrast, enabling easier fabrication. A discussion addressing optical resolution, printed part resolution, and their relationship to structure type has been added (line 319):

"Various factors influence the experimental printing resolution, such as the projection methods, the non-linear response of the materials, and the structures of target products. High-precision dose distributions of 11 μm have been observed in fluorescent solutions and relief-structure printouts of DISH (Figs. 4a-b and Supplementary Fig. 9). However, our experiments, alongside relevant literature[23], indicate that isolated small structures require much higher dose contrast and are sensitive to the surrounding dose distribution, highlighting the need for more precise dose control. Currently, we have achieved about 19 μm overall printing resolution across the effective depth range and 12 μm as the finest independent positive feature (Fig. 4). Algorithms that can increase dose contrast or take diffusion into consideration may further improve the overall printing resolution near the optical diffraction limit."

To characterize printed structures volumetrically, we reprinted the Theodoric model and conducted a CT scan using a Zeiss Xradia 620 Versa system; these results have been updated in Fig. R29 (Fig. 10h). For unsupported structures in this model, deformation during post-processing cannot be completely avoided. For instance, the deformation at the end of the left rod introduces additional mismatch between the printed structures and the original model. The root mean square (RMS) of the signed distance for the CT-scanned model is 45.7 μm; an RMS value larger than the resolution is a common occurrence in such volumetric characterizations.

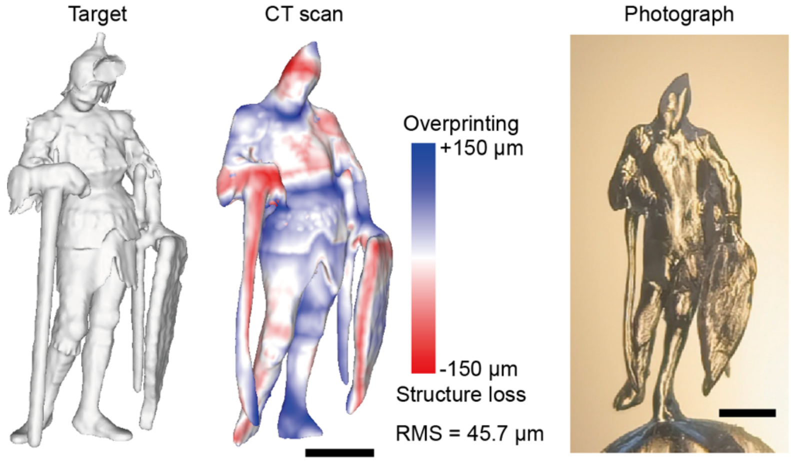

Figure R29: CT scan of the Theodoric sample (Fig S10h). The target model, the model reconstructed by CT scanning of the printed sample, and the image of the sample are demonstrated. The signed distances relative to the target model are visualized by color. Deformation of unsupported structures during post-processing led to additional accuracy loss. The final RMS of the signed distance is measured to be 45.7 μm. Scale bar: 1 mm.

As to the resolution value we used to describe the resolution of tomography-based 3D printing methods, the smallest printed feature sizes were also searched in those papers, regardless of their structures or materials (some materials shrink like dehydrated hydrogels or sintered glass). Although the resolution accuracy of tomography-based printing cannot be the same as those point-wise and layer-wise methods that have fixed resolution, Fig. R30 (Fig. S1) is made in an unbiased way.

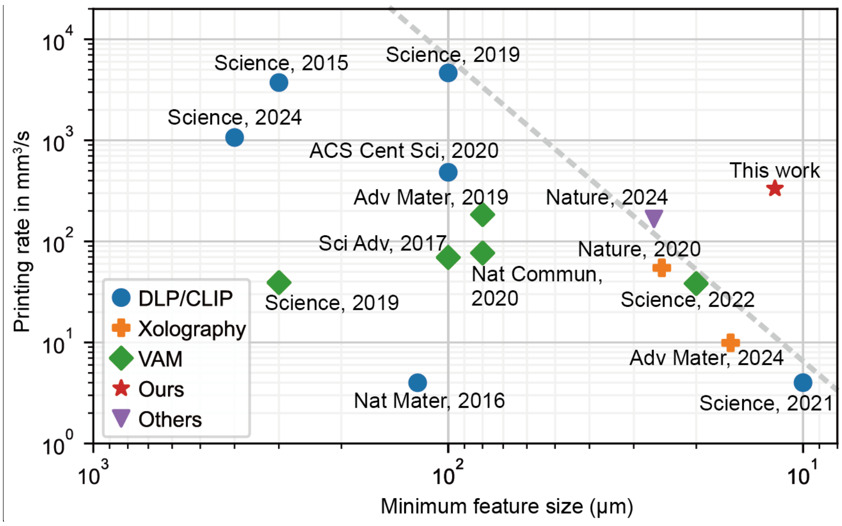

Figure R30: Benchmarking of DISH and state-of-the-art 3D printing methods. (**Fig. S1**) The gray dashed line in the figure represents a voxel efficiency of approximately 6.5×10^6 voxels/s, estimated under the assumption that the voxels in these works are cubes with side lengths equal to the minimum feature size. Our system achieves a voxel efficiency of

1.25×10^8 voxels/s, exhibiting advantages among printing methods of the same scale.

4) Shape fidelity and mechanical properties of printed objects:
To better convince the reader of the DISH process's performance, I would recommend including an image of the 3D model (e.g., STL file or similar) in Figure 1b, ideally placed side-by-side with a photograph of the printed object for a direct comparison of shape fidelity.

Throughout the manuscript, I found no information regarding the mechanical stability of the objects after printing and the subsequent post-processing step. The induced crosslinking may be sufficient to remove the object from the resin but might leave the construct soft and unstable. Photographs alone typically do not provide enough insight into this aspect. I suggest including an additional supplementary video that demonstrates the post-cured objects, which would also help visualize shape fidelity.
Furthermore, there is limited information provided in the Methods section on page 24 regarding the post-processing procedure. For instance, details on the irradiance (W/cm^2) and illumination time used during the 405 nm UV post-curing step would be helpful.

Response:

We sincerely appreciate the reviewer's comment. An image of the target model has been added to Fig. 1b and shown below.

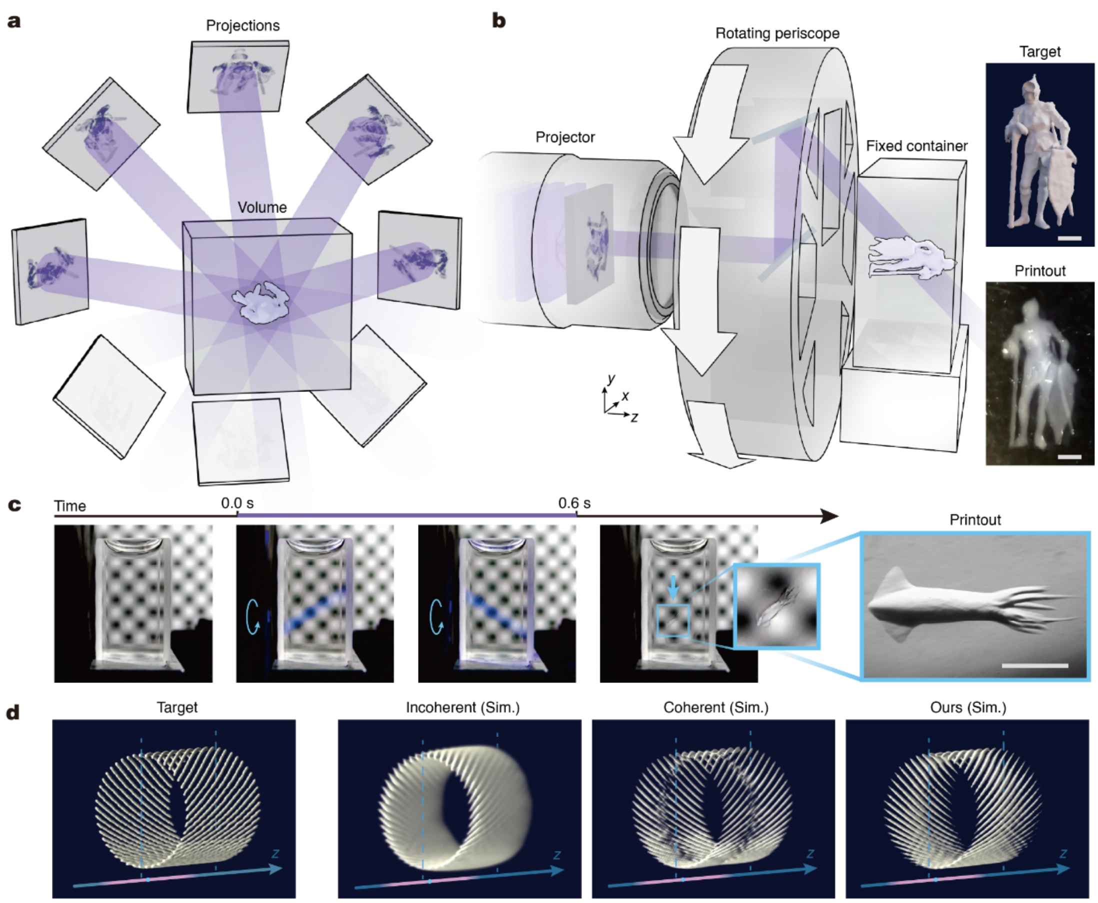

Figure R31 Principle and illustration of DISH. (Fig.1) a, Multi-angle projection is used to generate 3D light intensity distributions within a fixed container for volumetric printing. **b**, A rotating periscope is designed to generate a high-speed projection of the holographic patterns modulated by a digital mirror device (DMD) within 0.6 seconds. The product was imaged in water. **c,** Images at different time points showing that the printing process in a low-viscosity PEGDA aqueous solution can be finished within 0.6 seconds. **d,** Comparisons of the simulated 3D light distributions generated by DISH system with incoherent light, coherent light without holographic optimization, and coherent light with holographic optimization. The target ground truth is also shown on the left. Scale bar: 1 mm.

Most printed products from our system exhibit viable mechanical strength, allowing direct retrieval from the printing medium using a pipette or tweezers. Supplementary Videos 3 and 4 demonstrate that PEGDA structures printed with an exposure time of less than one second can be directly taken out with a tweezer or a pipette just after exposure. These products maintain their original shape when rinsed in water and gently squeezed. Notably, the mechanical strength of printed parts is strongly dependent on material properties and exposure parameters; it is also feasible to fabricate softer, low-crosslink density samples by adjusting the material composition, projection patterns, and exposure duration.

Additional details on post-processing have been added to the Methods section (line 561). After the samples are thoroughly rinsed in water or alcohol, they are supplemented with light using a 405nm beam at 30 mW/cm² for approximately 60 seconds front and back in photointiator solution (water containing 0.25% LAP or ethanol containing 2mM TPO). The deformation of unsupported features (e.g., the Theodoric sculpture) may be partly caused by this uneven exposure, since we noticed even in a commercialized 3D printer, printouts may deform in the matched post-processing chamber. Future work to build a post-processing chamber with uniform light in all directions for small and unsupported objects would be really helpful for extensive applications.

5) Holographic optimization

As is well-established from previous CAL studies, extensive modeling and algorithm development are required to compute projections for printing high-resolution, true-to-shape objects.

Based on the description in the Methods section, I assume that the algorithms published in references 25 and 26 are used to calculate coarse image projections (grayscale, real-valued) for N = 180 discrete angles. Is that correct? From each of these images, a set of G = 10 binarized images is generated, which are then processed through the holographic optimization algorithm, resulting in a total of 1800 projection images. Why not calculate projections directly for N = 1800 different angles using traditional algorithms, binarize them, and then feed them into the newly developed optimization algorithm? If the mentioned computation time is the reason for this approach, how long do these computations take to run on the machines used?

Additionally, I was searching for documentation regarding the software implementation of the PM methods and the Gerchberg-Saxton algorithm used in this work. For transparency, it would be helpful to provide more detailed information about the software and its implementation.

Response:

We sincerely appreciate the reviewer's comments. It is correct that we reproduced the Penalty Minimization approach described in the paper, *High Fidelity Volumetric Additive Manufacturing,* in the coarse optimization, with adjustments in beam propagation. We have provided additional details regarding the implementation of both the coarse optimization and the Global GS algorithm below. Additionally, we conducted simulations to obtain the fidelity of generating 1800 images first and then using a holographic algorithm to produce 1800 binary images. The results indicate that the performance of this method is inferior to that achieved with a higher binarization parameter *G*.

The coarse optimization step is based on the PM approach outlined in *High Fidelity Volumetric Additive Manufacturing*; our modification focuses on the projection calculation, that is, the relationship between dose and projection patterns. In ray optics, dose exhibits a linear relationship with projection patterns for any projection directions. By modeling ray-optic projection via real-valued matrix multiplication, different projection systems can utilize the same loss function and be solved using consistent mathematical formulations.

The coarse optimization adopting the PM method corresponds to the code https://github.com/sugar10w/DISH/blob/main/main_Adam_reinf.m
In this code, we manually implemented the Adam optimizer to optimize the loss function of

$$L = \sum_{\vec{x}\in A} |d_h - Hv|^2 + \sum_{\vec{x}\in \tilde{A}} |Hv - d_l|^2$$

where v denotes the vector composed of projection patterns from all viewing angles, and H is a matrix representing the linear process of ray-optic projection. The derivative of the loss function is

$$\mathrm{d}L/\mathrm{d}v = \mathcal{H}^{-1}\left[\sum_{\vec{x}\in A}(\mathcal{H}v - d_h) + \sum_{\vec{x}\in \tilde{A}}(\mathcal{H}v - d_l)\right]$$

The Global Gerchberg-Saxton algorithm used for comparison corresponds to the code https://github.com/sugar10w/DISH/blob/main/util/project/my_pb_gs_fres.m
As a foundational holographic method, the Global Gerchberg-Saxton algorithm infers a reasonable 3D phase through iterative projections: (1) Compute the projection $\mathcal{H}_\varphi V_\varphi$, and extract the phase of projected 3D complex amplitudes $\phi(\mathcal{H}_\varphi V_\varphi)$. (2) Combine the target 3D intensity with the inferred phase to obtain $\sqrt{I_\varphi} \cdot \phi(\mathcal{H}_\varphi V_\varphi)$. (3) Back-propagate each layer of complex amplitudes and superimpose them to generate a projection pattern $V_\varphi{}'$. (4) Apply device constraints to $V_\varphi{}'$ to obtain the updated V_φ. This process is repeated iteratively, and the optimal V_φ is selected as the output.

Computing 1800 viewing angles, followed by the holographic algorithm to obtain 1800 binary images, is similar to setting the binarization parameter *G*=1 in our algorithm. We have supplemented the fidelity performance corresponding to this parameter via simulations, as indicated by the arrow in Fig. R32:

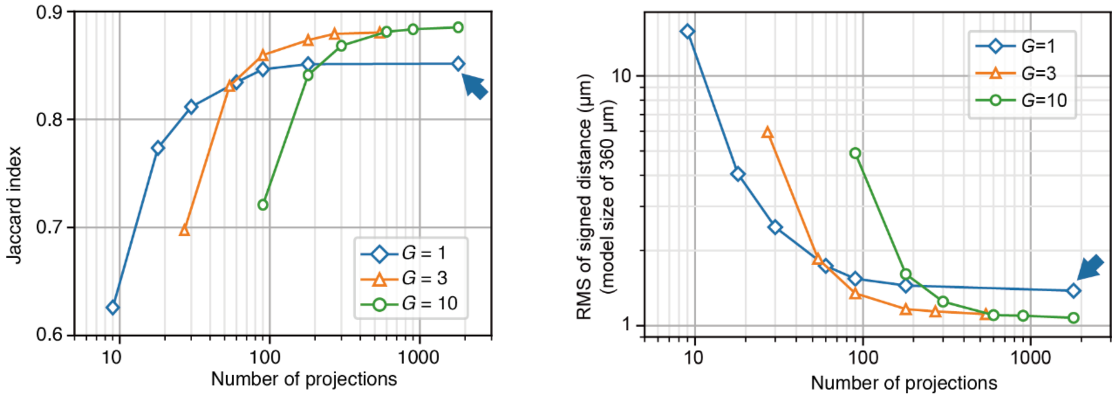

Figure R32: Numerical fidelity performance of calculating N=1800 views followed by G=1 binarization. The fidelity performance (Jaccard index and RMS of signed distance) for the process of computing 1800 viewing angles, followed by the holographic algorithm to obtain 1800 binary images has been supplemented. For the same total number of views, the fidelity of this setup is lower than that of setups using a higher binarization parameter (*G*).

For the test model, it is evident that simply increasing the number of projections yields only a marginal performance improvement, whereas adjusting the binarization parameter leads to a more significant enhancement. This is because fitting real-valued projections using multiple binary projections enables better approximation of diverse grayscale levels, resulting in higher projection fidelity than using a single binary projection per viewing angle.

6) Other points:

In the introduction on page 3 of the manuscript, the authors wrote: "Efforts have been made on continuous printing to enhance the production rate and reduce the layering structure, such as continuous liquid interface production, Xolography, and their improved versions for continuous production using continuous roll or fluid control. Still, the throughputs of these methods are fundamentally limited by the layer-wise process, especially for millimeter-scale or centimeter-scale objects."

Xolography is not a layer-wise process, as the material volume in relation to the vat remains stationary while the light-sheet moves continuously through the resin, resulting in smooth, highly homogeneous structures. Therefore, Xolography is a form of volumetric additive manufacturing, and this distinction should be reflected in the text.

Figure 1 provides a clear visualization of the illumination geometry (Fig. 1a,b) and a time series of the printing process (Fig. 1c). Fig. 1d displays a fine mesh structure, and at first glance, the reader may assume this is a printed object. However, the figure caption clarifies that it is a simulation. I would suggest that real prints and simulation data of different objects not be mixed within a single figure to avoid any confusion.

The cited literature list is well-constructed. However, a recent review article published in Nature may be worth including:

Bernal, P.N., Florczak, S., Inacker, S. et al. The road ahead in materials and technologies for volumetric 3D printing. Nat Rev Mater (2025). https://doi.org/10.1038/s41578-025-00785-3

Response:

We thank the reviewer for pointing out this problem. We incorrectly referred to Xolography as "layer-wise," as it also requires time for each layer, or more precisely, the light sheet scanning cannot be greatly sped up because the dual-color photoinitiator requires time to revert to the initial state that does not absorb the second-color light. Otherwise, the UV-initiated layer, or the visible light transparent layer of the material, might not be thin enough to maintain the designed depth and impair the printing.

The description of Xolography has been corrected as a form of volumetric additive manufacturing, and the regarding text is: "Xolography[15] is a form of volumetric additive manufacturing that moves a light sheet through the stationary resin. Despite its recent update with continuous production using fluid control system[16], the dual-color photoinitiator requires necessary time to revert, which restricts its volumetric build rates." (line 49)

The labels of Fig. 1d have added "(Sim.)" to avoid confusion. The updated figure is also shown in the comment "4) Shape fidelity and mechanical properties of printed objects" part.

The reference to *The road ahead in materials and technologies for volumetric 3D printing* has been added as [22].

Response to Referees

We sincerely thank the reviewers and editors for their insightful comments and constructive feedback on our manuscript entitled "Sub-second Volumetric Additive Manufacturing by Digital Incoherent Synthesis of Holographic Light Fields." We have thoroughly revised the manuscript in response to all concerns and provide below a detailed, point-by-point response. Additions and major changes in the revised manuscript are indicated by highlighting in red. For ease of communication, the original referee comments are shown in black color, whereas our specific answers are in blue. Thank you again for your great efforts.

Referee #1 (Remarks to the Author)

This manuscript by X. Wang & colleagues improves significantly upon the first submitted version of this paper. The work demonstrates four major advancements for volumetric additive manufacturing (VAM). 1. The fastest VAM print times reported to-date, 2. Optical access from only one side of the print volume, 3. Improved precision using holographic processing of the light fields, and 4. Stop-flow sequential production of dozens of distinct and varied parts.

Once again, I am impressed by the authors' careful, detailed responses to the reviewers and by their extensive characterization and depth of analysis of their system. In my view, the revised manuscript has sufficiently addressed all of the important concerns from all reviewers. From a technical/scientific perspective, the work is a tour-de-force that certainly merits speedy publication.

I will limit my remaining comments here to only those that aim to improve the clarity of the information presented in the manuscript so as to better convey to readers the key insights, conclusions, and impact of this work. I have one major suggestion, and a few minor suggestions.

Response:

We sincerely thank the referee for the detailed comments and the acknowledgment of our revision. We have revised our manuscript to improve the clarity as required by the referee. We have added the explanations of using an amplitude-modulation equipment to project light-field patterns, which are optimized holographically. Also, the figure demonstrating the binarization-induced error was incorporated as Extended Data Fig. 4b, and all the minor revisions were addressed as suggested.

INCOHERENT HOLOGRAPHIC SYNTHESIS

If I have correctly understood the authors' responses to reviewers, they do not claim that their hardware is capable of phase modulation. The DMD device is controlled to project binary intensity patterns, as is typical. Rather their key insight is that it's important to model the propagating optical fields using full-wave optics including amplitude and phase, and to treat their interaction and interference holographically, taking this into account for optimizing the distribution of light energy. This leads to more accurate dose estimation and better contrast optimization for the projected light fields, in addition to an extended region of precise optical pattern synthesis far outside the depth of focus of the objective. This is a subtle, but critical aspect of this work.

I believe it is important to convey this to readers using more precise language than currently present in the manuscript. There are a few phrases which imply that the hardware system is somehow holographically shaping the light patterns. These include "continuous multi-angle holographic projections" (line 29), "generate holographic patterns" (line 78), "using holographic light fields" (line 122), "operated with holographical patterns" (line 442), "projection of the holographic patterns" (line 732). The conventional understanding of all such phrases is that the hardware is capable of modulating the phase of the projected light fields, thereby generating holographic patterns. I recommend revising each of these phrases to avoid leaving this impression. On line 29, the word "holographic" can be simply omitted, and can be likewise omitted on line 78 as well, or replaced with "binary intensity." On line 122, I would suggest revising to "… we address this problem by using a coherent laser source, and holographically calculating the light fields, which can achieve …." On line 442, I suggest revising to "holographically synthesized patterns," and on line 732 revising to "… high-speed projection of the light patterns modulated by…."

I would also suggest explicitly stating somewhere (similarly to the authors responses to Reviewer 1) that indeed the hardware does not modulate the phase of the projected patterns, but calculating the propagation and interference of the light patterns holographically is critical to the success of this work. Perhaps this might fit well on line 80, before the sentence starting with "An iterative algorithm…"

Response:

We sincerely appreciate the referee's insightful comments and constructive suggestions. We have modified the texts as suggested by the reviewer to avoid potential misunderstanding. On the one hand, more precise phrases were chosen, and the language was revised as suggested by the reviewer (lines 29, 77, 122, 629, 469). On the other hand, direct statements were added at line 80: "Although DMD cannot directly modulate the phase of light field, we develop an iterative algorithm with the wave-optics propagation model and a customized loss function to optimize the projected light fields holographically for high-resolution 3D modulation with enhanced fidelity compared to traditional algorithms."

OTHER MINOR SUGGESTED REVISIONS

- It would be very helpful to include Figure R6 perhaps in the Supplementary Information, as a clear demonstration of the difference in pattern contrast due to binarization and why it needs to be included in the optimization loop.

Response:

We sincerely appreciate the referee's comment. Figure R6 has now been added as Extended Data Fig. 4b. In addition, the corresponding illustration has also been added in "Methods - Holographic optimization algorithm" section as: "Notably, directly converting a grayscale projection into a sequence of binary projections results in degraded intensity contrast out of the focal planes, because the light beams projected at different time points lack coherence to each other." (line 671)

- The sentence that begins on Line 34 of the abstract could better be worded as: "Acrylate resins in a range of viscosities are used to demonstrate…
- On line 69, the words "within snapshot" should be deleted.

Response:

We thank the referee for careful suggestions. The abstract has been revised as "Acrylate materials in a range of viscosities" and the phrase "within snapshot" was deleted.

- "Rounds" on lines 76, 99, and 310 should be replaced by "rotations." While on the topic, what is the actual rotation speed of the periscope during prints? The videos seem to show slower speed than 10 Hz.

Response:

We sincerely appreciate the referee's correction. The words have been replaced by "rotations".

The practical speed of the periscope is 0.6 seconds per rotation, as demonstrated in supplementary videos. The system did not operate at the fastest speed, mainly due to the limited laser intensity. In addition, our current experimental setup requires additional acceleration time to reach its maximum rotating speed of 10 Hz.

An explanation has been added at line 571: "Since the laser power used in our current prototype system is relatively low, all trigger parameters described here are specifically configured for the 0.6-second exposure time rather than for maximum operating speed."

- On line 202 "calibration" should be "calibrate"
- On line 213 "tripe" should be "triple"
- On line 288, "an" is missing before "elastic"
- On line 476, the sentence should begin "It satisfies the condition that…"

Response:

We sincerely thank the referee for pointing out these mistakes. We have corrected accordingly.

- On line 486, I suggest revising to "The incoherent synthesis more accurately represents our experimental implementation...

Response:

We appreciate the referee's comments. This sentence was revised accordingly.

- The sentences between lines 512-516 need to be proofread for language usage and corrected

Response:

We thank the referee for the careful suggestion. We have carefully revised this part, deleted the less relevant descriptions, and added details about the printing chemicals. The revised text is: "The enhanced scattering makes the printouts more visible, and the printing process can thus be directly captured by cameras. In addition, binary solvents could induce faster polymerization than a single solvent[51,] and faster curing is suitable for DISH." (line 703) The full names of the chemicals "PEGDA 1000" and "PEG 400" have been supplemented at their first occurrence in this section.

Referee #2 (Remarks to the Author):

The authors have done a very good job revising the manuscript and clearing up the remaining questions. As stated originally, this paper is an important advancement in the field of Volumetric Additive Manufacturing which merits publication in Nature. The reviewer recommends acceptance for publication at this point. There are a few more points which would be of interest but none of them merit further delay of publication at this point. Very well done!

Referee #2 (Remarks on code availability):

The code is well documented and the logic is clear.

Response: We sincerely thank the referee for the great efforts and the positive comments on our work and improvements.